



**HAL**  
open science

## Multiple sources for tephra from AD 1259 volcanic signal in Antarctic ice cores

Biancamaria Narcisi, Jean Robert Petit, Barbara Delmonte, Valentina Batanova, Joel Savarino

► **To cite this version:**

Biancamaria Narcisi, Jean Robert Petit, Barbara Delmonte, Valentina Batanova, Joel Savarino. Multiple sources for tephra from AD 1259 volcanic signal in Antarctic ice cores. *Quaternary Science Reviews*, 2019, 210, pp.164-174. 10.1016/j.quascirev.2019.03.005 . hal-02350371

**HAL Id: hal-02350371**

**<https://hal.science/hal-02350371v1>**

Submitted on 25 Nov 2020

**HAL** is a multi-disciplinary open access archive for the deposit and dissemination of scientific research documents, whether they are published or not. The documents may come from teaching and research institutions in France or abroad, or from public or private research centers.

L'archive ouverte pluridisciplinaire **HAL**, est destinée au dépôt et à la diffusion de documents scientifiques de niveau recherche, publiés ou non, émanant des établissements d'enseignement et de recherche français ou étrangers, des laboratoires publics ou privés.

## Manuscript Details

**Manuscript number** JQSR\_2019\_21  
**Title** MULTIPLE SOURCES FOR TEPHRA FROM AD 1259 VOLCANIC SIGNAL IN ANTARCTIC ICE CORES

### Abstract

Strong volcanic signals simultaneously recorded in polar ice sheets are commonly assigned to major low-latitude eruptions that dispersed large quantities of aerosols in the global atmosphere with the potential of inducing climate perturbations. Parent eruptions responsible for specific events are typically deduced from matching to a known volcanic eruption having coincidental date. However, more robust source linkage can be achieved only through geochemical characterisation of the airborne volcanic glass products (tephra) sometimes preserved in the polar strata. We analysed fine-grained tephra particles extracted from layers of the AD 1259 major bipolar volcanic signal in four East Antarctic ice cores drilled in different widely-spaced locations of the Plateau. The very large database of glass-shard geochemistry combined with grain size analyses consistently indicate that the material was sourced from multiple distinct eruptions. These are the AD 1257 mega-eruption of Samalas volcano in Indonesia, recently proposed to be the single event responsible for the polar signal, as well as a newly-identified Antarctic eruption occurred in AD 1259. Finally, a further eruption that took place somewhere outside Antarctica has contributed to tephra deposition. Our high-resolution, multiple-site approach was critical to reveal spatial heterogeneity of tephra at the continental scale. Evidence from ice-core tephra indicates recurrent explosive activity at the Antarctic volcanoes and could have implications for improved reconstruction of post-volcanic effects on climate from proxy polar records.

### Submission Files Included in this PDF

#### File Name [File Type]

AD1259\_text\_Jan\_2019.docx [Manuscript File]

Fig1\_sample position\_dic18.pdf [Figure]

figura 2\_v3.JPG [Figure]

Fig3\_micro foto dic 2018.pdf [Figure]

Fig4\_TAS\_AD1259\_thin+ comp.pdf [Figure]

Fig5\_TASthin\_trend TD.pdf [Figure]

Supplementary\_AD1259\_rev2019.docx [MethodsX]

To view all the submission files, including those not included in the PDF, click on the manuscript title on your EVISE Homepage, then click 'Download zip file'.

### Research Data Related to this Submission

There are no linked research data sets for this submission. The following reason is given:  
Microprobe single-grain data are given as Supplementary Material along with details of analytical conditions

# MULTIPLE SOURCES FOR TEPHRA FROM AD 1259 VOLCANIC SIGNAL IN ANTARCTIC ICE CORES

Biancamaria Narcisi<sup>1</sup>, Jean Robert Petit<sup>2</sup>, Barbara Delmonte<sup>3</sup>, Valentina Batanova<sup>4</sup>, Joël Savarino<sup>2</sup>

(1) ENEA, C.R. Casaccia, 00123 Roma, Italy, biancamaria.narcisi@enea.it

(2) Univ. Grenoble Alpes, CNRS, IRD, Grenoble INP, IGE, 38000 Grenoble, France

(3) Department of Earth and Environmental Sciences (DISAT), Univ. Milano-Bicocca, Piazza della Scienza, 20126 Milano, Italy

(4) Univ. Grenoble Alpes, Univ. Savoie Mont Blanc, CNRS, IRD, IFSTTAR, ISTERre, 38000 Grenoble, France

## Abstract

Strong volcanic signals simultaneously recorded in polar ice sheets are commonly assigned to major low-latitude eruptions that dispersed large quantities of aerosols in the global atmosphere with the potential of inducing climate perturbations. Parent eruptions responsible for specific events are typically deduced from matching to a known volcanic eruption having coincidental date. However, more robust source linkage can be achieved only through geochemical characterisation of the airborne volcanic glass products (tephra) sometimes preserved in the polar strata. We analysed fine-grained tephra particles extracted from layers of the AD 1259 major bipolar volcanic signal in four East Antarctic ice cores drilled in different widely-spaced locations of the Plateau. The very large database of glass-shard geochemistry combined with grain size analyses consistently indicate that the material was sourced from multiple distinct eruptions. These are the AD 1257 mega-eruption of Samalas volcano in Indonesia, recently proposed to be the single event responsible for the polar signal, as well as a newly-identified Antarctic eruption occurred in AD 1259. Finally, a further eruption that took place somewhere outside Antarctica has contributed to tephra deposition. Our high-resolution, multiple-site approach was critical to reveal spatial heterogeneity of tephra at the continental scale. Evidence from ice-core tephra indicates recurrent explosive activity at the Antarctic volcanoes and could have implications for improved reconstruction of post-volcanic effects on climate from proxy polar records.

35 **Highlights**

- 36 • Significant tephra concentration in AD 1259 volcanic signal from four Antarctic ice cores  
37 • Compositional heterogeneity of tephra suggests sourcing from multiple distinct eruptions  
38 • Linkage of the Antarctic ice signal with the Samalas AD 1257 eruption confirmed  
39 • A new Antarctic eruption that occurred in AD 1259 has been also identified  
40 • Antarctic regional-scale effects of local volcanic activity conceivable

41 **Key words:** Cryptotephra; Antarctica; Ice Cores; Volcanic isochron; Glass shard  
42 microanalysis; Antarctic rifting volcanism; Samalas AD 1257 eruption

## 43 1. Introduction

44

45 As ~~it is~~ documented in the vast literature produced during the last four decades, continuous  
46 volcanic profiles from polar ice sheets reconstructed by electric conductivity (ECM) and  
47 sulphate measurements are punctuated by prominent spikes recording explosive eruptions  
48 of the past (e.g., Hammer, 1980; Delmas et al., 1992; Langway et al., 1995; Severi et al., 2012;  
49 Sigl et al., 2014, 2015). These signals can be used both as reference horizons to provide  
50 independent age constraints for the ice core series, and to reconstruct the history of  
51 explosive volcanism and its relationship with climate. Volcanic events with bipolar  
52 occurrence are particularly interesting in this respect. These are typically interpreted as  
53 related to massive low-latitude events capable to produce sulphuric acidic deposition all  
54 over the world with the potential of forcing global climate (e.g., Langway et al., 1995; Sigl et  
55 al., 2015). Their record in both polar regions also enables direct north-south synchronisation  
56 of ice stratigraphies, which is of crucial importance to reconstruct the phasing of climatic  
57 events and understanding underlying mechanisms (Svensson et al., 2013).

58 Among the most outstanding volcanic deposition events of the last 2 millennia (Sigl et al.,  
59 2014), peak fallout of volcanic aerosols over the poles dated ~~AD~~ 1259 represents a  
60 fundamental age marker for ice chronologies. Its signal is recorded in several Greenland and  
61 Antarctic ice cores, and was initially identified by Langway et al. (1988), who suggested that  
62 the parent volcano could be probably located in the Northern Hemisphere close to Equator.  
63 Since then, numerous papers have considered various aspects of this event (e.g. Delmas et  
64 al., 1992; Zielinski, 1995; Stothers, 2000). Particularly, its source has been a matter of debate  
65 as until recently no record of large volcanic eruption around that date was known. On the  
66 basis of analysis of tiny glass shards, Palais et al. (1992) suggested that the material from  
67 Greenland and South Pole (SP) ice levels is indeed from the same volcano, and identified El  
68 Chichón, Mexico, as the probable source, despite the chemical match was not perfect in  
69 detail. Oppenheimer (2003) presented the hypothesis of a super-eruption of global  
70 significance or a smaller eruption enriched in sulphur. Baroni et al. (2008) used sulphur  
71 isotope analysis to indicate a stratospheric nature for the volcanic signals at the Antarctic  
72 Dome C and SP sites. More recently, a major caldera explosive event was identified at  
73 Samalas volcano, on Lombok Island, Indonesia (Lavigne et al., 2013, Vidal et al., 2015, 2016;  
74 Alloway et al., 2017). Based upon chronostratigraphic and geochemical studies nearby the  
75 source, and the analysis of historical texts, this eruption of exceptional size was dated at AD  
76 1257, placed at the end of the Medieval Warm Period (ca. 900-1250 A.D., Mann et al., 2009). It  
77 has been inferred to be the single counterpart of the AD 1259 bipolar spike. In particular,  
78 according to a recent reconstruction of Antarctic continental-scale volcanic aerosol  
79 deposition, the sulphate injection greatly exceeded that of the AD 1815 cataclysmic Tambora  
80 eruption (Sigl et al., 2014).

81 When strong explosive volcanic eruptions occur, large quantities of solid particles (tephra)  
82 and gases penetrate the tropopause and rise to altitudes well within the stratosphere, where  
83 they can be distributed all around the globe. Tephra fallout can affect vast regions, and small  
84 particles can be deposited thousands of kilometres from active sources forming invisible  
85 horizons (e.g., Lowe, 2011; Ponomareva et al., 2015, and references therein). The fingerprint  
86 of volcanic material preserved in distant sites can univocally identify source areas and could  
87 be employed to disentangle the origin of volcanic glacio-chemical signals in polar ice cores

88 (e.g., Yalcin et al., 2006; Dunbar et al., 2017), that otherwise is conjectured from the record of  
89 documented eruptions. However, especially for tropical-equatorial eruptions the amount of  
90 tephra that could be dispersed towards the poles is typically very small and the material very  
91 fine-grained, making such tephra study very challenging.

92 A preliminary exploratory investigation of a shallow Antarctic ice core from the Concordia-  
93 Dome C site revealed evidence of an appreciable concentration of cryptotephra in  
94 connection with the AD 1259 sulphate peak (Petit et al., 2016). This intriguing observation  
95 prompted us to carry out a detailed tephra study in order to make inferences about source(s)  
96 that produced the tephra and to discuss the related atmospheric implications. In this work  
97 we describe the characteristics of the glassy volcanic material associated with the AD 1259  
98 signal in different sectors of the East Antarctic Plateau (EAP). We took advantage of having  
99 access to various good-quality ice cores covering the last millennium to apply a multiple core  
100 approach that allows highlighting the spatial distribution of volcanic products. Note that  
101 while attempts to identify the parent eruption of major polar signals through a tephra study  
102 often rely on few shards (e.g., Zielinski et al., 1997; Barbante et al., 2013), here we obtained a  
103 large dataset based on a considerable amount of electron probe microanalyses that allows  
104 recognizing compositional heterogeneities within tephra, in association with ash grain size  
105 measurements. We also considered an inventory of candidate source volcanoes more  
106 extended than that employed in previous studies.

## 107 **2. Materials and Methods**

108 In this study we used 4 EAP ice cores located at elevations between 1950 and 3488 m (Figure  
109 1 and Table S1). Two core sites, Dome C-Concordia (DC) and Vostok (VK), are located ~ 600  
110 km apart in the central, inner sector of the Plateau, and two, Talos Dome-TALDICE (TD) and  
111 GV7, are ~ 200 km apart in peripheral position facing the Ross Sea. They show different  
112 modern climate and atmospheric characteristics (e.g., Masson-Delmotte et al., 2011) as well  
113 as distance from the Quaternary volcanoes of the Antarctic rift provinces. All the cores used  
114 have an undisturbed stratigraphy and are provided with a detailed volcanic aerosol profile,  
115 either as sulphate or ECM measurements. They all show the broad and pronounced signal  
116 unambiguously related to the AD 1259 event that occurs at variable depth depending on the  
117 accumulation rate of the site (between 29.6 m at VK and 181.9 m at GV7, Figure 1a).

118 Since at the visual core inspection no macroscopic evidence for the presence of tephra was  
119 detected, the core depth intervals corresponding to the volcanic spike were sub-sampled  
120 continuously, albeit with different resolution (5 to 15 cm) depending on the local  
121 accumulation rate. Processing of subsamples for laboratory measurements was carried out  
122 under clean conditions. To reduce contamination of samples to a minimum, the outer  
123 portion of porous firn samples was removed with a clean ceramic knife while ice pieces were  
124 washed thrice in ultrapure water. The resulting decontaminated samples were then melted  
125 and an aliquot was used for quantitative measurements of dust concentration and size  
126 distribution using a Coulter Counter set up in a class 100 clean room (Delmonte et al., 2002).  
127 The only exception relates to the GV7 core, where presence of abundant drilling fluid  
128 prevented accurate Coulter Counter measurements. A separate aliquot of meltwater from  
129 levels showing unusually high concentration of particles with respect to the local background  
130 was filtered (nucleopore polycarbonate membranes) for tephra recovery. Filters were  
131 examined using light and scanning electron microscopes, and typical tephra grains were

132 photographed (Figure 2). To investigate the source for the recovered material, we  
133 determined the major element composition of individual shards using the electron  
134 microprobe set up at the Institut des Sciences de la Terre (ISTerre) of Grenoble. The  
135 operating details are given in the Supplementary Material.

136 From the initial geochemical dataset (over 900 analyses) collected during different sessions,  
137 we cautiously discarded analytical data showing total oxide sums  $\leq 60\%$  and those obviously  
138 related to pure minerals (quartz, plagioclase, metals, etc.). The rest, consisting  $\sim 320$   
139 measurements generally made on very small individual glass particles, was normalised to  
140 100% total oxide values for subsequent interpretation. We expect a decrease of precision but  
141 after normalisation all the elements with oxide contents  $> 1\%$  can be considered robust  
142 enough for interpretation (Iverson et al., 2017).

### 143 3. Results

144 EAP core samples selected at the culmination of the volcanic spike show microparticle  
145 concentrations well above background levels for each site (Fig. 2). Central Plateau samples  
146 show concentrations higher (a factor 6 to 10) than background levels for firn ( $\sim 8$  ppb,  
147 Delmonte et al., 2013) and mass size distributions well-defined around modal values smaller  
148 than background ( $\sim 2 \mu\text{m}$  on average during Holocene, Delmonte et al., 2005). For DC, the  
149 mode is around  $1.7 \mu\text{m}$ , while for VK it is between  $1.3 \mu\text{m}$  and  $1.9 \mu\text{m}$  respectively for samples  
150 VK-16 and VK-14, although some very large particles up to  $\sim 20 \mu\text{m}$  were included in the  
151 latter.

152 TD sample 87-1 from the base of the volcanic sulphate peak shows very large particles with  
153 mass modal values as high as  $\sim 6 \mu\text{m}$ , associated concentration levels higher than  $\sim 10$   
154 times background levels for firn ( $\sim 12$  ppb, Delmonte et al., 2013). From the lowermost to the  
155 uppermost part of the volcanic spike (see Figure 1a for stratigraphic position of the samples),  
156 a progressive decrease in microparticle concentration and size can be observed. A  
157 population of particles larger than  $\sim 5 \mu\text{m}$  is present in the two deepest samples (TD 87-1 and  
158 86-4), while the relative abundance of particles smaller than  $2 \mu\text{m}$  increases upward within  
159 the peak. We note that sample 86-4 shows a bimodal distribution with a first mode smaller  
160 than  $2 \mu\text{m}$  and a larger mode around  $4\text{-}6 \mu\text{m}$ .

161 At the microscopic inspection, glass particles generally display well-preserved textures with  
162 no traces of abrasion strongly suggesting that the material was not subject to reworking  
163 (Figure 3). Among the examined samples, TD 87-1 and 86-4 contain pumice particles with  
164 elongated vesicles up to ca.  $40\text{-}50 \mu\text{m}$  long along with fine-size shards remnants of thin  
165 vesicle walls. Particles in the filters from the inner EAP cores are typically represented by tiny  
166 curved and platy-like shards. Material from sample VK-14 contains glass particles up to  $15\text{-}20$   
167  $\mu\text{m}$  in size. Microscopic observations coupled with grain size analysis exclude that the  
168 volcanic material belongs to background dust, and instead provide compelling evidence of  
169 primary tephra deposition at levels within the AD 1259 acidity peak.

170 Results of grain-specific geochemical analysis are illustrated in Figs 4-5, where the data are  
171 plotted on the total alkali-silica (TAS) diagram. Silica co-variations with  $\text{K}_2\text{O}$ ,  $\text{CaO}$ ,  $\text{FeO}$  and  
172  $\text{Al}_2\text{O}_3$ , not shown here, are coherent in providing the same chemical pattern. Representative  
173 analyses of individual glass shards are presented in Table S3, along with biplot comparisons

174 of selected major-oxide ratios in the present data and in published literature for further  
175 potential source volcanoes and equivalents (Supplementary Material).

176 The analysed glass shards, taken altogether, display variable silica contents, from  
177 intermediate to evolved compositions ( $\text{SiO}_2 > 52$  wt %). No basic and ultrabasic  
178 geochemistries are represented. Within the glass heterogeneous composition spreading over  
179 three TAS fields, we identify two main separate clusters of data, one trachytic falling in the  
180 alkaline field,  $\sim 63\text{-}65$  wt %, and the other showing sub-alkaline affinity and straddling the  
181 trachyte-dacite-rhyolite boundaries (for brevity referred to hereafter as 'dacitic'),  $\sim 70$  wt %. A  
182 third subpopulation, subordinate in terms of frequency, shows a siliceous rhyolitic  
183 composition ( $\text{SiO}_2 > 74$  wt %).

184 Volcanic glass composition also varies spatially (Figure 4a). Ice core shards from the Central  
185 EAP sites are predominantly sub-alkaline in composition. However, the three analysed  
186 samples display different characteristics. The very fine-grained DC sample and sample VK-14  
187 also dominantly dacitic. Sample VK-16 displays two clusters of geochemical data. The main  
188 glass population is dacitic in composition and appears comparable with that in sample VK-14  
189 and in DC, the subordinate population is a siliceous rhyolite. Sparse analyses from both VK  
190 samples fall within the trachytic glass group.

191  
192 In all six ice sections from the two peripheral EAP sites trachytic tephra particles are  
193 dominating, but with occurrence of subordinate glass with different signature (Fig. 4a). At TD,  
194 we observe an interesting compositional variation with respect to the time-stratigraphic  
195 position of the samples (Figure 5). Volcanic ash on the TD 87-1 filter, situated at the very  
196 beginning of the sulphate fallout (Figure 1) and containing coarse particles, is mainly  
197 trachytic in composition. The adjacent TD 86-4 from the acme of the sulphate volcanic signal  
198 shows two main coexisting glass populations. This is consistent with the striking bimodal  
199 grain size distribution of this sample (Figure 2). According to scanning electron microscopic  
200 check during microprobe analysis, coarser particles correspond to trachyte, finer particles  
201 are mostly dacitic. Glass from the upper TD 86 samples -3 and -2, stratigraphically located at  
202 the later part of the spike and populated by fine particles, is trachytic. GV7 ice shows co-  
203 existing trachytic and dacitic geochemistries (Figure 4a). The two analysed samples are  
204 equally heterogeneous (not shown). In all samples from the peripheral cores, only one shard  
205 from TD falls within the rhyolite cluster identified in VK-16 (Figure 4a).

206

## 207 **4. Interpretation and discussion**

208

### 209 *4.1 Identification of tephra sources*

210

211 Filters from all studied cores contain significant volcanic glass that appears heterogeneous  
212 both in grain size and geochemistry and present variable spatial characteristics.

213 Taken as a whole, the composition of glass shards allows two prevailing and a third  
214 subsidiary populations to be distinguished. Trachytic shards are more abundant in the  
215 samples from peripheral EAP sites, which are characterised by coarser grain size. Dacitic  
216 shards occur in all sites but are dominating in the Central EAP samples, typically  
217 characterised by smaller particle size. This pattern ~~already~~ suggests that tephra transport



218 and deposition could be controlled by different atmospheric dynamics over the Plateau.  
219 Although tephra transport is very different from background dust input onto the EAP (Narcisi  
220 et al., 2005), mineral dust investigations highlighted that the periphery of the ice sheet ~~in fact~~  
221 is influenced by regional atmospheric circulation dynamics of the Western Ross Sea, while  
222 sites from the inner part of the EAP are more sensitive to long-range high-altitude transport  
223 above Antarctica (e.g., Delmonte et al., 2013).

224 Focusing on the geochemical signature of volcanic glass as a major criterion for source  
225 identification, we first point out that compositional heterogeneity in a tephra horizon could  
226 be related to magmatic differentiation during a single parent explosive episode or to coeval  
227 deposition from separate events. Several examples of both types of tephra are known in  
228 Antarctic ice (e.g., Narcisi et al., 2016). Since alkaline (i.e. trachytic) composition and sub-  
229 alkaline (i.e. dacitic) composition typically pertain to different tectonic settings, here we  
230 interpret co-existing trachytic and dacitic tephtras in the studied samples as related to  
231 contemporaneous eruptions from independent sources.




232 Alkaline trachytic compositions are characteristic of Antarctic volcanoes, belonging to one of  
233 the largest active alkali rift systems of the world (Werner, 1989). Indeed, the identified  
234 trachytic glass shards, particularly copious in the filters from peripheral cores that are  
235 adjacent to Victoria Land volcanic provinces, is chemically very consistent with compositions  
236 of the tephra layers in the TALDICE core originated from local sources during the last climatic  
237 cycle (Narcisi et al., 2012, 2016, 2017) (Figure 4b). We therefore deduce that the trachytic  
238 glass in the studied samples was produced by a local Antarctic explosive eruption occurred at  
239 AD 1259. The coarse particle size observed at TD which is ~ 200 km distant from the inferred  
240 source area, further supports this interpretation. This event dispersed material mostly over  
241 the adjacent ice sheet region, but the ash deposition involved also more inland areas of the  
242 EAP, as the occurrence of sporadic trachytic shards in the VK samples demonstrates.  
243 Infrequent ash layers of Antarctic derivation in long cores from the EAP have been already  
244 observed within the last four glacial-interglacial cycle ice series (e.g., Narcisi et al., 2010). We  
245 infer that the Antarctic volcanic plume entered into the polar vortex circulation and then  
246 rapidly reached the inner sectors of the Plateau. Based on the available data, it is unclear  
247 whether the plume from the AD 1259 Antarctic eruption dispersed particulate material onto  
248 the SP area. In the early tephra investigation by Palais et al. (1992), no trace of trachytic glass  
249 is reported for the Antarctic ice core. That tephra study however, was based upon the  
250 analysis of a handful of volcanic particles, representing a limitation for the detection of  
251 compositional heterogeneity and multiple fingerprints within individual horizons. Finally,  
252 similarly to other local eruptions, this Antarctic event likely delivered sulphate aerosols, but  
253 this is difficult to detect as it is combined with the coincidental broad signal peaking at AD  
254 1259 related to long-range stratospheric transport and deposition of aerosols and generated  
255 during an extra-Antarctic source event (see discussion below). Note that examples of circa-  
256 coeval multiple eruptions manifesting as a single volcanic signal are known in the Antarctic  
257 ice record (Cole-Dai and Mosley-Thompson, 1999; Cole-Dai et al., 2000). They represent tricky  
258 case studies for estimation of atmospheric aerosol loadings by related eruptions, with  
259 implications for assessment of the real impact on climate (e.g., Timmreck et al., 2009).

260 Our discovery of Antarctic-sourced tephra associated with the AD 1259 acidic deposition is  
261 remarkable given the postulated tropical source of the eruption responsible for this polar





262 signal (e.g., Sigl et al., 2015). Nevertheless it is not particularly surprising considering that  
263 Antarctic volcanoes from Victoria Land and Marie Byrd Land show evidence of Holocene-  
264 historical activity and ice cores drilled adjacent to volcanoes contain numerous locally  
265 derived discrete tephra layers, sometimes in the form of invisible horizons, as a result of  
266 persistent explosive activity (e.g., Kurbatov et al., 2006; Narcisi et al., 2012). In this respect,  
267 we point out that that the local eruption identified here does not correspond to the Antarctic  
268 event dated  $1254 \pm 2$  AD that produced widespread tephra deposition over most of the  
269 Pacific-facing sector of Antarctica (Narcisi and Petit, 2018, and references therein). At TD and  
270 GV7 in fact this eruption occurs as both coarse visible ash and a sharp sulphate spike  
271 standing well above the background values and clearly preceding the AD 1259 volcanic peak  
272 (e.g., Narcisi et al., 2001; Severi et al., 2012). The newly identified event neither corresponds  
273 to the local eruption at AD 1261 detected as both volcanic sulphate deposition and a large  
274 particle concentration peak in the West Antarctic Ice Sheet (WAIS) Divide ice core (Koffman et  
275 al., 2013) that clearly follows the AD 1259 signal. Therefore, within a decade three distinct  
276 local events took place in the Antarctic mainland that left tangible fallout traces in the ice  
277 sheet. Such rapid succession of eruptions could be overlooked in low time resolution studies  
278 and instead needs to be carefully considered when addressing the attribution of Antarctic  
279 ice-core signals, as having implications for reconstructions of volcanic forcing.

280 The main sub-alkaline component of dacitic composition is genetically linked to subduction-  
281 related volcanism. Differently from the trachytic glass, it is not straightforward to identify the  
282 source responsible for this tephra. The distant geographic location of the EAP with respect to  
283 subduction provinces provides no clues, and the tiny particle size of the volcanic material in  
284 the Central EAP ice suggests long-distance transport, thus enlarging the suite of potential  
285 source areas to be considered to the whole Southern Hemisphere and even beyond the  
286 Equator. Note in this respect that although not very frequently, ash produced in equatorial-  
287 tropical volcanoes could have reached Antarctica during past eruptions, as in the case of  
288 Pinatubo (15°14'N) tephra (2-10  $\mu\text{m}$ ) identified in the 1993-94 snow layers at South Pole after  
289 the 1991 eruption (Cole-Dai et al., 1997). In the search for possible sources for the dacitic  
290 tephra, we therefore considered an extended inventory of volcanoes. A thorough discussion  
291 of this piece of our work is presented in Supplementary Material.

292 The recently discovered volcanic eruption of Samalas in the Indonesian Archipelago (8°33'S)  
293 was suggested as the most probable source for the AD 1259 polar spike, due to its  
294 exceptional size (estimated VEI and maximum plume height 7 and 43 km, respectively) and  
295 appropriate date (e.g., Lavigne et al., 2013; Vidal et al., 2015, 2016; Alloway et al., 2017).  
296 Indeed, we found ~~a~~ positive chemical match with Samalas products over all constituent  
297 elements considered (Figure 4b). Thus, the striking geochemical similarities between the  
298 Samalas glass and the ice core dacitic glass population along with the significant differences  
299 between the ice core glass and products from other potential sources (Figure S2) led us to  
300 conclude that our dacitic glass material was sourced from the Samalas AD 1257 eruption.  
301 Note that this volcanic material is also chemically coherent with glass shards formerly found  
302 in Greenland and SP ice cores (Palais et al., 1992) suggesting a common source eruption  
303 (Figure 4b). The cataclysmic AD 1257 Samalas explosive eruption clearly ranks among the  
304 greatest volcanic events of the Holocene. Once injected into the stratosphere up to about 40  
305 km (Vidal et al., 2015), the Samalas tephra particles must have been transported poleward.  
306 Volcanic particles are supposed to settle in the lower stratosphere and accumulate just

307 above the tropopause, similarly to  $^{10}\text{Be}$  and sulphate. Then, when stratosphere/troposphere  
308 exchange of mass and chemical species occurs above Antarctica, sedimentation of volcanic  
309 aerosols proceeds within the troposphere  at the ice sheet surface. The whole process  
310 likely occurred on a timescale of 1-2 years, as indicated by the time shift between the  
311 eruption and deposition. Evidence for stratospheric transport of volcanic ash to Central EAP  
312 in association with strong explosive eruptions is not new. At Vostok, it has been observed  
313 (Delmonte et al., 2004) that small particles with modal values around 1.5-1.7  $\mu\text{m}$  are  
314 generally associated  stratospheric ash entering the troposphere during  
315 stratosphere/troposphere folding, jointly with sulphate and likely  $^{10}\text{Be}$ . We believe that in   
316 case of injection of large quantities of volcanic ash to great heights in the stratosphere also  
317 some relatively large particles can be transported in the stratosphere at great distance from  
318 the source, as suggested by presence of some large dacitic glasses in VK-14 sample.

319 A limited subset of glass analyses from a Vostok sample indicate distinctive high-silica  
320 rhyolitic composition with sub-alkaline affinity (Figure 4a). In the TAS diagram, this evolved  
321 component appears separated from the two main glass populations previously discussed,  
322 suggesting a different source. Note that this rhyolitic glass was not detected in the samples  
323 from the peripheral sites characterised by conspicuous deposition of locally-originated  
324 trachytic ash, suggesting that it is likely unrelated to the newly identified Antarctic eruption.  
325 Indeed, no such composition is known in the recent volcanic record from Antarctic centres  
326 (Dunbar et al., 2008; Narcisi et al., 2012) and neither in the Samalas products (Vidal et al.  
327 2015; Alloway et al., 2017). We therefore infer that this glass could be originated from a  
328 further distant event that contributed to the ice-core tephra. Interestingly, this interpretation  
329 could be in accordance with previous investigations in the WAIS Divide ice core that show  
330 that the stratospheric microparticle deposition during the year 1258 occurred in two pulses  
331 (Koffman et al., 2013), thus hinting for the possible contribution of two quasi-coeval tropical  
332 volcanic eruptions.

333 In the Southern Hemisphere, rhyolitic products related to subduction processes occur at  
334 some active Andean volcanoes and especially in the volcanic centres of New Zealand ( $\sim 39^\circ\text{S}$ ,  
335 ca. 6000 km from the Vostok site in direct line), whereas rarely were erupted from West  
336 Antarctic intraplate volcanoes . Rhyolitic ice-core glass shards display higher  $\text{K}_2\text{O}$  contents  
337 compared to glasses of **American**  contemporary volcanoes; they are also characterised by  
338  $\text{CaO}$  and  $\text{FeO}$  contents  $< 1 \text{ wt}\%$ , more typical of New Zealand rhyolitic glasses than of the  
339 Antarctic (Marie Byrd Land) ones found in the marine realm (Shane and Froggatt, 1992)  
340 (Figure S3). Although we are aware that some Andean centres may have been more  
341 geochemically evolved than ~~it is currently represented in literature data~~ , none of the  
342 considered volcanoes appear compositionally ~~coherent with~~  our ice-core tephra sub-  
343 population (Figure S3).

344 Considering the recent tephra record of New Zealand volcanoes, we observe that ice-core  
345 glass mimics the chemical composition of Kaharoa Tephra, which represents the only  
346 rhyolitic deposit during the last 1000 years in the region (Nairn et al., 2004, Lowe et al., 2013)  
347 (Figure S3). This plinian eruption however is precisely dated to  $\text{AD } 1314 \pm 12$  (Lowe et al.,  
348 2013, and references therein), thus is ca. 50 years younger than the polar spike (Lowe and  
349 Higham, 1998). Therefore, despite the geochemical similarities, the significant age difference  
350 prevents this correlation. We conclude that the source for the identified rhyolitic glass, likely

351 located outside the Antarctic continent, remains undecided. Nevertheless, the New Zealand  
352 volcanic province represents the most frequently active rhyolitic zone on Earth (e.g., Smith et  
353 al., 2005) and is a suitable source of tephra in Antarctica, despite only one New Zealand  
354 tephra layer in Antarctic ice has been identified so far (Dunbar et al., 2017). Our intriguing  
355 finding could hopefully provide a hint for future investigations.

#### 356 357 4.2 Implications

358  
359 Volcanic eruptions are drivers of transient weather and climate disturbances (e.g., Robock,  
360 2000). The possible climate-forcing produced by the Samalas event, the most powerful  
361 eruption of the last millennium, has been addressed in several papers using various proxy  
362 archives and historical documents, along with estimate of the release of gas during the  
363 eruption based upon an independent geochemical approach. The volatile emissions standing  
364 as the greatest volcanogenic gas injection of the last few millennia were enough to produce  
365 global cooling (Vidal et al., 2016). Indeed, considerable environmental and social post-  
366 volcanic effects were reconstructed that along the Central Indonesian archipelago affected  
367 also vast regions of Europe (Guillet et al., 2107; Alloway et al., 2017). According to Gennaretti  
368 et al. (2014), tree-ring-based temperature reconstruction from northeastern North America  
369 displays an abrupt cooling regime shift that chronologically coincides with the occurrence of  
370 a series of eruptions centred around the AD 1257 Samalas event suggesting volcanic impact  
371 on the local forests and ice-caps. Moreover, indirect geological sources show occurrence of  
372 an El Niño-like event in the Americas and SE Asia in the year after the mega-eruption that  
373 suggests causal connection between the volcanic event and the climate anomaly (Emile-  
374 Geay et al., 2008; Alloway et al., 2017). In the Antarctic record, the 13<sup>th</sup> century appears  
375 exceptionally rich in conspicuous volcanic signals, with the AD 1259 being the most  
376 prominent (e.g., Cole-Dai et al., 2000). Possible effects of volcanic activity around the date of  
377 1259 have been invoked also for high southern latitudes, but the data are still very sparse.  
378 Using a combination of firn/ice core records, Frezzotti et al. (2013) identified middle 13<sup>th</sup>  
379 century as the onset of a 50yrs-long period of negative surface mass balance of the Antarctic  
380 ice sheet at the continental scale. This pattern could be related to solar irradiance with other  
381 factors, as volcanic forcing, superimposing (Frezzotti et al., 2013).

382 Results of ice-core tephra studies presented here and elsewhere (Koffman et al., 2013; Narcisi  
383 and Petit, 2018, and references therein) collectively have shown for the first time that three  
384 distinct Antarctic eruptions took place in the time span of a decade between AD 1254 ± 2 and  
385 AD 1261. These eruptions produced deposition of tephra blanket and atmospheric sulphate  
386 aerosols onto the polar ice sheet. In the ice volcanic record local eruptions typically emitting  
387 only tropospheric sulphate are represented by strong but short-lived residence times of  
388 aerosols in the atmosphere (e.g., Castellano et al., 2005). This pattern suggests that such  
389 individual events most likely are incapable of significant large-scale climatic impact.  
390 However, here we raise question about the potential consequences of this closely spaced  
391 local eruption sequence occurred in association with the tropical Samalas eruption, on the  
392 Antarctic climate and environment. Note that owing to the close proximity to the source  
393 region the local forcing would be exerted through both the radiative impacts of gas and  
394 particulate aerosols and the reduction in ice surface albedo produced by repeated extensive  
395 tephra deposition. With respect to the latter factor, recent estimations have shown the  
396 significance of volcanic ash deposition onto snow/ice even from mid-sized eruptions at high-

397 latitudes to alter surface reflectivity and enhance glacier melting (e.g., Dacic et al., 2013;  
398 Young et al., 2014; Muschitiello et al., 2017). Given the continuous sustained explosive activity  
399 of the Antarctic volcanoes with related large production of tephra and consequent dispersal  
400 over the Plateau due to favourable atmospheric conditions (e.g., Scarchilli et al., 2011), we  
401 believe that the potential role of forcing caused by locally-derived ash deposits should not be  
402 neglected in Antarctic palaeoclimate reconstructions. This factor deserves further more  
403 specific investigation in future research.

404 With respect to sulphate emission, unfortunately the available data currently do not permit  
405 to distinguish between the contribution to the aerosol deposition from the Samalas event  
406 and the AD 1259 local Antarctic eruption. These limitations notwithstanding, at this stage we  
407 can remark that in Antarctica two distinct volcanic forcings (one tropical and the other of  
408 high southern-latitude) may be superimposed around the date of 1259. In conclusion, our  
409 results add complexity to interpretation of volcanic aerosol yields from polar records and  
410 could have implications for more reliable climate model simulations for the pre-instrumental  
411 period (Schneider et al., 2009; Stoffel et al., 2015, and references therein).

## 412 5. Conclusions

413 Non-visible tephra deposits trapped within polar snow and ice represent precious  
414 chronostratigraphic tools. When the material is found associated with a prominent acidic  
415 signal, firm attribution to specific eruptions can be given with implications for climate forcing  
416 reconstructions. However, tephra detection and fingerprinting such remote locations is  
417 often problematic. We successfully used four cores collected from different sites in the EAP to  
418 demonstrate extensive deposition of volcanic dust on the ice sheet coeval with the large  
419 acidity peak at AD 1259, a key time stratigraphic horizon of inter-hemispheric significance.  
420 Our compelling data show that the material displays different characteristics from site to  
421 site. Geochemical fingerprinting of tephra, obtained with a grain-specific methodology,  
422 indicates that altogether multiple distinct explosive events have contributed to the ice core  
423 ash deposition, i.e. a newly-identified Antarctic eruption in AD 1259, the great AD 1257  
424 eruption of Samalas, and a further eruption likely occurred somewhere outside Antarctica.  
425 Indeed, spatial variations reflecting different atmospheric circulation patterns over the EAP  
426 were significant in the volcanic deposition on the ice sheet and should not be discounted in  
427 order to obtain sound source attribution of volcanic signals in polar sequences. We therefore  
428 underline the need of detailed studies based upon a multi-site and parameter approach as  
429 well as a large number of chemical analyses for capturing complexities inside tephra. Our  
430 results of the chemical composition of hundreds of microscopic particles confirm the inferred  
431 linkage of the Antarctic ice signal with the Samalas tropical eruption occurred in AD 1257, but  
432 also provide evidence for a coincidental cluster of local explosive events, so far not  
433 adequately considered in climate reconstructions derived by ice-core volcanic aerosol  
434 records. Local activity instead was important in shaping the Antarctic volcanic record and  
435 should be regarded as an agent of potential regional disturbances, not least through  
436 dispersion of ash over large areas with consequent radiative impact. We emphasise the  
437 potential of tephra investigations with respect to traditional measurements of aerosol  
438 concentrations in ice also for identifying superimposition of distinct contemporary events at  
439 a single site. Our findings also contribute to a more complete reconstruction of the history of  
440 volcanic activity in the Antarctic region.

441 **Aknowledgements**

442

443 We thank D.J. Lowe (University of Waikato) for his useful advice on New Zealand  
444 tephrochronology, N. Metrich and J.-C. Komorowski (Institut de Physique du Globe de Paris)  
445 for providing tephra samples from the Samalas deposits, C. Rado for drilling operations at  
446 Vostok, and E. Gautier (IGE, Grenoble) for DC ice sample selection. The Vostok ice core was  
447 obtained during 1991-92 field season through the Russian US French collaboration on ice  
448 cores with the support from the Soviet-Russian Antarctic Expedition, the National Science  
449 Foundation and the French Polar Institute. This works contributes to TALos Dome Ice CorE  
450 (TALDICE), a joint European programme lead by Italy and funded by national contributions  
451 from Italy, France, Germany, Switzerland and the United Kingdom, that was aimed at  
452 retrieving an ice core reaching back through the previous two interglacials (about 250,000  
453 years). This is TALDICE publication no. xxx.. The GV7 drilling project, carried out in  
454 cooperation with KOPRI (Korea Polar Research Institute), was financially supported by the  
455 MIUR (Italian Ministry of University and Research)-PNRA (Italian Antarctic Research  
456 Programme) program through the IPICS-2kyr-It project. Author Contributions: B.N. and J.R.P.  
457 conceived this study. J.R.P. conducted ice-core sample processing grain-size analysis, and  
458 preliminary microprobe work. B.N. conducted tephra analysis, interpreted the results, and  
459 wrote most of the manuscript. V.B. was responsible for microprobe work. B.D. interpreted  
460 grain-size data and significantly contributed to the writing of the text. J.S. collaborated in the  
461 discussion of the experimental results.

462 **Figure captions**

463 Figure 1. (a) AD 1259 signal (as sulphate in mg/L, or electrical conductivity, ECM, in arbitrary  
464 units) in the studied Antarctic cores. TALDICE sulphate profile redrawn from Severi et al.  
465 (2012), GV7 sulphate profile courtesy of R. Nardin. Also shown is the position of samples  
466 analysed for grain size and geochemistry (grey shaded blocks). The dashed line indicates  
467 'bag' section limit and/or core break. (b) Map of Antarctica with location of the ice cores and  
468 main Quaternary volcanoes in Victoria Land (e.g., Mt. Erebus, Mt. Melbourne and The  
469 Pleiades) and in Marie Byrd Land, West Antarctica (e.g., Mt. Takahe and Mt. Berlin).

470 Figure 2. Mass-size distributions (Relative Units, R.U., %) of samples analysed for  
471 geochemistry. (A): Central EAP samples from Dome C (DC 71-a) and Vostok BH6 (VK-30-14 and  
472 VK-30-16) ice cores. (B): TD samples 87-1, 86-4, 86-3, 86-2 from the base to the top of the  
473 volcanic sulphate spike.

474  
475 Figure 3. Scanning electron microphotographs of volcanic glass particles from a, DC-71a; b-c,  
476 VK-14; d-e, TD-87-1; f, TD-86-4.

477 Figure 4. (a) Total alkali-silica (TAS) classification diagram and alkaline/sub-alkaline division  
478 line (Rickwood, 1989, and references therein) showing the normalised analyses of ice-core  
479 shards. Ph= Phonolite, An = Andesite, T = Trachyte, D = Dacite, Rh = Rhyolite. In the inset the  
480 TAS diagram with envelopes for the three glass compositional sub-populations is illustrated.  
481 (b) The TAS classification diagram as above showing the whole data set (in grey-scale)  
482 compared with glass geochemical analyses for the most likely correlatives (data from  
483 Alloway et al., 2017; Narcisi et al., 2012, 2016, 2017; Palais et al., 1992). Geochemical  
484 comparison with further potential sources is provided in Supplementary Material.

485 Figure 5. Total alkali-silica (TAS) classification diagram and alkaline/sub-alkaline division line  
486 (Rickwood, 1989, and references therein) for the normalised analyses of ice-core shards in  
487 the four TD samples. Data of pertinent samples are superimposed upon the whole data set  
488 (in grey-scale) for comparative purposes. Ph = Phonolite, An = Andesite, T = Trachyte, D =  
489 Dacite, Rh = Rhyolite. For the stratigraphic position of samples with respect to the AD 1259  
490 ice-core volcanic signal see Fig. 1.

491  
492 **Captions for Supplementary Tables and Figures**

493 Table S1. Location and characteristics of the studied ice cores.

494 Table S2. Composition of reference glasses and Samalas samples measured at different  
495 analytical conditions.

496  
497 Table S3. Representative major element composition of individual glass shards determined  
498 by electron microprobe analysis. Values are given in weight % oxide and are normalised to  
499 100%. Total iron is expressed as FeO. MnO not determined. Glass populations as defined in  
500 the main text.

501  
502 Figure S1. World map showing the location of Antarctic ice core sites (blue dots) and of

503 selected volcanic sources considered in the text (red triangles). Letters for sources are as  
504 follows. CH, Chaitén; EC, El Chichón; HU, Hudson; MBL, Marie Byrd Land; NZ, New Zealand;  
505 PCC, Puyehue-Cordon Caulle; QU, Quilotoa; SM, Samalas; SSh, South Shetland Islands; SSI,  
506 South Sandwich Islands; VL, Victoria Land.

507 Figure S2. Monte Carlo simulation of the interaction and emission volumes of X-rays at 10kV  
508 for Na-K $\alpha$  in Na-Si rich glass considered as A) common polished sample and B) small 1x1  $\mu$ m  
509 particle placed on the C-glue. The blue lines show the electron trajectory outside the particle.

510  
511 Figure S3. Major element biplots for the analysed ice-core shards (in grey-scale) compared  
512 with glass geochemical analyses for selected potential sources and counterparts (data from  
513 Moreno et al., 2015; Fontijn et al., 2016; Nairn et al., 2004; Kratzmann et al., 2009; Moreno et  
514 al., 2015; Nooren et al., 2017; Stewart and Castro, 2016; Shane and Froggatt, 1992). Location  
515 of considered source volcanoes is shown in Supplementary Figure S1.



516 **References**

- 517  
518 Alloway, B.V., Andreastuti, S., Setiawan, R., Miksic, J., Hua, Q. (2017). Archaeological implications of a  
519 widespread 13th Century tephra marker across the central Indonesian Archipelago. *Quaternary Science Reviews*  
520 155, 86-99, <https://doi.org/10.1016/j.quascirev.2016.11.020>
- 521 Barbante, C., Kehrwald, N. M., Marianelli, P., Vinther, B. M., Steffensen, J. P., Cozzi, G., Hammer, C. U., Clausen, H.  
522 B., Siggaard-Andersen, M.-L. (2013). Greenland ice core evidence of the 79 AD Vesuvius eruption. *Climate of the*  
523 *Past* 9, 1221-1232, <https://doi.org/10.5194/cp-9-1221-2013>
- 524 Baroni, M., Savarino, J., Cole-Dai, J., Rai, V.K., Thiemens, M. H. (2008). Anomalous sulfur isotope compositions of  
525 volcanic sulfate over the last millennium in Antarctic ice cores. *Journal of Geophysical Research: Atmospheres*  
526 113, D20, 2156-2202, DOI: 10.1029/2008JD010185
- 527 Castellano, E., Becagli S., Hansson M., Hutterli M., Petit J.R., Rampino M.R., Severi M., Steffensen J.P., Traversi R.,  
528 Udisti R. (2005). Holocene volcanic history as recorded in the sulfate stratigraphy of the European Project for Ice  
529 Coring in Antarctica Dome C (EDC96) ice core. *Journal of Geophysical Research* 110, D06114,  
530 [doi:10.1029/2004JD005259](https://doi.org/10.1029/2004JD005259)
- 531 Cole-Dai, J., Mosley-Thompson, E., Thompson, L.G. (1997). Quantifying the Pinatubo volcanic signal in south  
532 polar snow. *Geophysical Research Letters* 24, 2679–2682.
- 533 Cole-Dai, J., Mosley-Thompson, E. (1999). The Pinatubo eruption in South Pole snow and its potential value to  
534 ice-core paleovolcanic records. *Annals of Glaciology* 29, 99-105. [doi:10.3189/172756499781821319](https://doi.org/10.3189/172756499781821319)
- 535 Cole-Dai, J., Mosley-Thompson, E., Wight, S. P., Thompson, L.G. (2000). A 4100-year record of explosive  
536 volcanism from an East Antarctica ice core. *Journal of Geophysical Research* 105(D19), 24431–24441,  
537 [doi:10.1029/2000JD900254](https://doi.org/10.1029/2000JD900254)
- 538 Dadic, R., Mullen, P.C., Schneebeli, M., Brandt, R.E., Warren, S.G. (2013). Effects of bubbles, cracks, and volcanic  
539 tephra on the spectral albedo of bare ice near the Transantarctic Mountains: Implications for sea glaciers on  
540 Snowball Earth. *Journal of Geophysical Research: Earth Surface*, 118, 1658-1676, [doi:10.1002/jgrf.20098](https://doi.org/10.1002/jgrf.20098)
- 541 Delmas, R.J., Kirchner, S., Palais, J.M., Petit, J.R. (1992). 1000 years of explosive volcanism recorded at the South  
542 Pole. *Tellus* 44B, 335-350.
- 543 Delmonte, B., Petit, J.R., Maggi, V. (2002). Glacial to Holocene implications of the new 27000-year dust record  
544 from the EPICA Dome C (East Antarctica) ice core. *Climate Dynamics* 18, 647-660, DOI 10.1007/s00382-001-0193-  
545 9
- 546 Delmonte, B., Petit, J.R., Andersen, K.K., Basile-Doelsch, I., Maggi, V., Lipenkov, V.Ya (2004). Dust size evidence  
547 for opposite regional atmospheric circulation changes over east Antarctica during the last climatic transition.  
548 *Climate Dynamics* 23 (3-4), 427-438.
- 549 Delmonte, B., Petit, J.R., Krinner, G., Maggi, V., Jouzel, J., Udisti, R. (2005). Ice core evidence for secular  
550 variability and 200-year dipolar oscillations in atmospheric circulation over East Antarctica during the Holocene.  
551 *Climate Dynamics*, 24 (6), 641-654.
- 552 Delmonte, B., Baroni, C., Andersson, P.S., Narcisi, B., Salvatore, M.C., Petit, J.R., Scarchilli, C., Frezzotti, M.,  
553 Albani, S., Maggi, V. (2013). Modern and Holocene aeolian dust variability from Talos Dome (Northern Victoria  
554 Land) to the interior of the Antarctic ice sheet. *Quaternary Science Reviews* 64, 76-89,  
555 <http://dx.doi.org/10.1016/j.quascirev.2012.11.033>
- 556 Dunbar, N.W., McIntosh, W.C., Esser, R.P. (2008). Physical setting and tephrochronology of the summit caldera  
557 ice record at Mount Moulton, West Antarctica. *Geological Society of America Bulletin* 120, 796–812, [doi:](https://doi.org/10.1130/B26140.1)  
558 <https://doi.org/10.1130/B26140.1>

- 559 Dunbar, N.W., Iverson, N.A., Van Eaton, A.R., Sigl, M., Alloway, B.V., Kurbatov, A.V., Mastin, L.G., Mc Donnell, J.R.,  
560 Wilson, C.J.N., (2017). New Zealand supereruption provides time marker for the Last Glacial Maximum in  
561 Antarctica. *Scientific Reports* 7, Article number: 12238, doi: 10.1038/s41598-017-11758-0
- 562 Emile-Geay, J., Seager, R., Cane, M.A., Cook, E.R., Haug, G.H. (2008). Volcanoes and ENSO over the past  
563 millennium. *Journal of Climate* 21, 3134-3148.
- 564 Frezzotti, M., Scarchilli, C., Becagli, S., Proposito, M., Urbini, S. (2013). A synthesis of the Antarctic surface mass  
565 balance during the last 800 yr. *The Cryosphere* 7, 303-319, <https://doi.org/10.5194/tc-7-303-2013>
- 566 Gennaretti, F., Arseneault, D., Nicault, A., Luc Perreault L., Bégin, Y. (2014). Volcano-induced regime shifts in  
567 millennial tree-ring chronologies from northeastern North America. *Proceedings of the National Academy of*  
568 *Sciences* 111 (28) 10077-10082; <https://doi.org/10.1073/pnas.1324220111>
- 569 Guillet, S., Corona, C., Stoffel, M., Khodri, M., Lavigne, F., Ortega, P. et al. (2017). Climate response to the  
570 Samalas volcanic eruption in 1257 revealed by proxy records. *Nature Geoscience* 10,123–128.  
571
- 572 Hammer, C.U. (1980). Acidity of polar ice cores in relation to absolute dating, past volcanism, and radio-echoes.  
573 *Journal of Glaciology* 25, 359-372, <https://doi.org/10.3189/S0022143000015227>  
574
- 575 Koffman, B.G. Kreutz K.J., Kurbatov, A.V., Dunbar, N.W. (2013). Impact of known local and tropical volcanic  
576 eruptions of the past millennium on the WAIS Divide microparticle record. *Geophysical Research Letters* 40, 1–5,  
577 doi:10.1002/grl.50822
- 578 Kurbatov, A.V., Zielinski, G.A., Dunbar, N.W., Mayewski, P.A., Meyerson, E.A., Sneed, S.B., Taylor, K.C. (2006). A  
579 12,000 year record of explosive volcanism in the Siple Dome Ice Core, West Antarctica. *Journal of Geophysical*  
580 *Research* 111, D12307, doi:10.1029/2005JD006072
- 581 Iverson, N.A., Kalteyer, D., Dunbar, N.W., Kurbatov, A.V., Yates, M. (2017). Advancements and best practices for  
582 analysis and correlation of tephra and cryptotephra in ice. *Quaternary Geochronology* 40, 45-55,  
583 <https://doi.org/10.1016/j.quageo.2016.09.008>  
584
- 585 Langway, C.C., Clausen, H., Hammer, C. (1988). An inter-hemispheric volcanic time-marker in ice cores from  
586 Greenland and Antarctica. *Annals of Glaciology* 10, 102–108.
- 587 Langway, C.C. Jr., Osada, K., Clausen, H.B., Hammer, C.U., Shoji, H. (1995). A 10-century comparison of  
588 prominent bipolar volcanic events in ice cores. *Journal of Geophysical Research* 100 (D8), 16241–16247.
- 589 Lavigne, F., Degeai, J.-P., Komorowski, J.-C., Guillet, S., Robert, V., Lahitte, P., Oppenheimer, C., Stoffel, M., Vidal,  
590 C.M., Surono, Pratomo, I., Wassmer, P., Hajdas, I., Sri Hadmoko, D., de Belizal, D. (2013). Source of the great A.D.  
591 1257 mystery eruption unveiled, Salamas volcano, Rinjani Volcanic Complex, Indonesia. *Proceedings of the*  
592 *National Academy of Sciences* 110 (42) 16742-16747, <https://doi.org/10.1073/pnas.1307520110>
- 593 Lowe, D.J., 2011. Tephrochronology and its application: a review. *Quaternary Geochronology* 6,107–153,  
594 <http://dx.doi.org/10.1016/j.quageo.2010.08.003>
- 595 Lowe, D.J., Blaauw, M., Hogg, A.G., Newnham, R.M. (2013). Ages of 24 widespread tephtras erupted since 30,000  
596 years ago in New Zealand, with re-evaluation of the timing and palaeoclimatic implications of the Lateglacial  
597 cool episode recorded at Kaipo bog. *Quaternary Science Reviews* 74, 170-194.
- 598 Lowe, D.J., Higham, T.F.G. (1998). Hit-or-myth? Linking a 1259 AD acid spike with an Okataina eruption.  
599 *Antiquity* 72, 427-431.
- 600 Mann, M.E., Zhang, Z., Rutherford, S., Bradley, R.S., Hughes, M.K., Shindell, D., Ammann, C., Faluvegi, G., Ni, F.  
601 (2009). Global signatures and dynamical origins of the Little Ice Age and Medieval Climate Anomaly. *Science* 326,  
602 1256–1260, DOI: 10.1126/science.1177303

603 Masson-Delmotte, V., Buiron, D., Ekaykin, A., Frezzotti, M., Gallée, H., Jouzel, J., Krinner, G., Landais, A.,  
604 Motoyama, H., Oerter, H., Pol, K., Pollard, D., Ritz, C., Schlosser, E., Sime, L.C., Sodemann, H., Stenni, B., Uemura,  
605 R., Vimeux, F. (2011). A comparison of the present and last interglacial periods in six Antarctic ice cores. *Climate*  
606 *of the Past* 7, 397–423.

607 Muschitiello, F., Pausata, F.S.R., Lea, J.M., Mair, D.W.F., Wohlfarth, B. (2017). Enhanced ice sheet melting driven  
608 by volcanic eruptions during the last deglaciation. *Nature Communications* 8, Article number: 1020, DOI:  
609 10.1038/s41467-017-01273-1  
610

611 Nairn, I.A, Shane, P.R, Cole, J.W, Leonard, G.J, Self, S., Pearson, N. (2004). Rhyolite magma processes of the ~AD  
612 1315 Kaharoa eruption episode, Tarawera volcano, New Zealand. *Journal of Volcanology and Geothermal*  
613 *Research* 131, 265-294, [https://doi.org/10.1016/S0377-0273\(03\)00381-0](https://doi.org/10.1016/S0377-0273(03)00381-0)

614 Narcisi, B., Proposito, M. Frezzotti, M. (2001). Ice record of a 13th century explosive volcanic eruption in northern  
615 Victoria Land, East Antarctica. *Antarctic Science* 13, 174-181.

616 Narcisi, B., Petit, J.R., Delmonte, B., Basile-Doelsch, I., Maggi, V. (2005). Characteristics and sources of tephra  
617 layers in the EPICA-Dome C ice record (East Antarctica): implications for past atmospheric circulation and ice  
618 core stratigraphic correlations. *Earth and Planetary Science Letters* 239, 253-265.  
619

620 Narcisi, B., Petit, J.R., Delmonte, B. (2010). Extended East Antarctic ice core tephrostratigraphy. *Quaternary*  
621 *Science Reviews* 29, 21–27.

622 Narcisi, B., Petit, J.R., Delmonte, B., Scarchilli, C., Stenni, B. (2012). A 16,000-yr tephra framework for the  
623 Antarctic ice sheet: a contribution from the new Talos Dome core. *Quaternary Science Reviews* 49, 52–63.

624 Narcisi, B., Petit, J.R., Langone, A., Stenni, B. (2016). A new Eemian record of Antarctic tephra layers retrieved  
625 from the Talos Dome ice core (Northern Victoria Land). *Global and Planetary Change* 137, 69-78,  
626 <http://dx.doi.org/10.1016/j.gloplacha.2015.12.016>

627 Narcisi, B., Petit, J.R., Langone, A., 2017. Last glacial tephra layers in the Talos Dome ice core (peripheral East  
628 Antarctic Plateau), with implications for chronostratigraphic correlations and regional volcanic history.  
629 *Quaternary Science Reviews*, 165, 111-126.  
630

631 Narcisi, B., Petit, J.R. (2018). Englacial tephra of East Antarctica. In J. Smellie, K. Panter, A. Geyer (eds),  
632 *Volcanism in Antarctica: 200 Million Years of Subduction, Rifting and Continental Break-Up*. Geological Society,  
633 London, Memoirs, in press.

634 Oppenheimer, C. (2003). Ice core and palaeoclimatic evidence for the timing and nature of the great mid-13th  
635 century volcanic eruption. *International Journal of Climatology* 23, 417–426, doi:10.1002/joc.891  
636

637 Palais, J.M, Germani, M.S., Zielinski, G.A. (1992). Interhemispheric transport of volcanic ash from a 1259 A.D.  
638 volcanic eruption to the Greenland and Antarctic ice sheets. *Geophysical Research Letters* 19(8), 801–804.

639 Petit, J.R., Narcisi, B., Batanova, V.G., Savarino, J., Komorowski, J.C., Michel, A., Metrich, N., Besson, P., Vidal, C.,  
640 Sobolev, A.V. (2016). Identifying the AD 1257 Salamas volcanic event from micron-size tephra composition in  
641 two East Antarctic ice cores. *Geophysical Research Abstracts*, 18, EGU2016-5191.

642 Ponomareva, V., Portnyagin, M., Davies, S.M. (2015). Tephra without borders: far-reaching clues into past  
643 explosive eruptions. *Frontiers in Earth Science* 3 (83), doi:10.3389/feart.2015.00083

644 Rickwood, P.C. (1989). Boundary lines within petrologic diagrams which uses oxides of major and minor  
645 elements, *Lithos* 22, 247-263.  
646

647 Robock, A. (2000). Volcanic eruptions and climate. *Reviews of Geophysics* 38, 191-219,  
648 doi:10.1029/1998RG000054

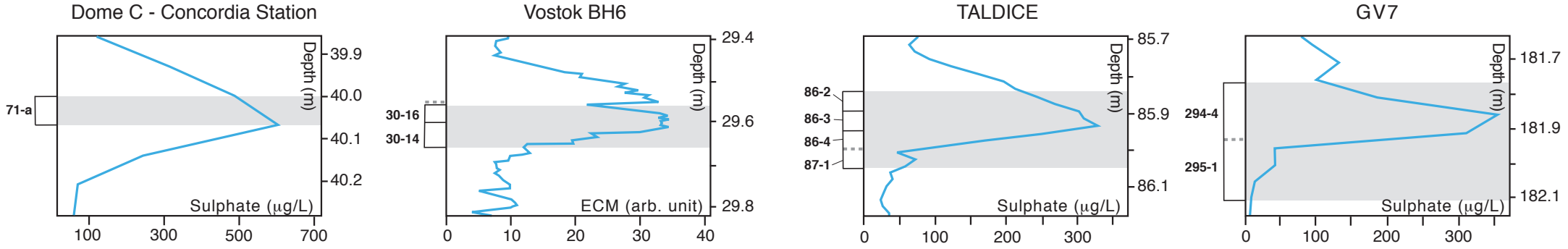
- 649 Scarchilli, C., Frezzotti, M., Ruti, P.M. (2011). Snow precipitation at four ice core sites in East Antarctica:  
650 provenance, seasonality and blocking factors. *Climate Dynamics* 37, 2107-2125,  
651 <http://dx.doi.org/10.1007/s00382-010-0946-4>.
- 652 Schneider, D. P., Ammann C. M., Otto-Bliesner B.L., Kaufman, D.S. (2009). Climate response to large, high-  
653 latitude and low-latitude volcanic eruptions in the Community Climate System Model. *Journal of Geophysical*  
654 *Research* 114, D15101, doi:10.1029/2008JD011222
- 655 Severi, M., Udisti, R., Becagli, S., Stenni, B., Traversi, R. (2012). Volcanic synchronisation of the EPICA-DC and  
656 TALDICE ice cores for the last 42 kyr BP. *Climate of the Past* 8, 509-517.
- 657 Shane, P.A.R., Froggatt, P.C. (1992). Composition of widespread volcanic glass in deep-sea sediments of the  
658 Southern Pacific Ocean: an Antarctic source inferred. *Bulletin of Volcanology* 54, 595-601.  
659
- 660 Sigl, M., McConnell, J.R., Toohey, M., Curran, M., Das, S.B., Isaksson, E., Kawamura, K., Kipfstuhl, S., Krüger, K.,  
661 Layman, L., Maselli, O.J., Motizuki, Y., Motoyama, H., Pasteris, D.R., Severi, M., (2014). Insights from Antarctica on  
662 volcanic forcing during the Common Era. *Nature Climate Change* 4, 693-697,  
663 <http://dx.doi.org/10.1038/nclimate2293>  
664
- 665 Sigl, M., Winstrup, M., McConnell, J.R., Welten, K.C., Plunkett, G., Ludlow, F., Büntgen, U., Caffee, M., Chellman,  
666 N., Dahl-Jensen, D., Fischer, H., Kipfstuhl, S., Kostick, C., Maselli, O.J., Mekhaldi, F., Mulvaney, R., Muscheler, R.,  
667 Pasteris, D.R., Pilcher, J.R., Salzer, M., Schüpbach, S., Steffensen, J.P., Vinther, B.M., Woodruff, T.E. (2015).  
668 Timing and climate forcing of volcanic eruptions for the past 2,500 years. *Nature* 523, 543-549.  
669 doi:10.1038/nature14565
- 670 Smith, V.C., Shane, P., Nairn, I.A. (2005). Trends in rhyolite geochemistry, mineralogy, and magma storage  
671 during the last 50 kyr at Okataina and Taupo volcanic centres, Taupo Volcanic Zone, New Zealand. *Journal of*  
672 *Volcanology and Geothermal Research* 148 (3-4), 372-406, <https://doi.org/10.1016/j.jvolgeores.2005.05.005>
- 673 Stoffel, M., Khodri, M., Corona, C., Guillet, S., Poulain, V. Bekki, S., Guiot J., Luckman B.H., Oppenheimer C.,  
674 Lebas, N., Beniston M., Masson-Delmotte V. (2015). Estimates of volcanic-induced cooling in the Northern  
675 Hemisphere over the past 1,500 years. *Nature Geoscience* 8, 784-788, DOI: 10.1038/NNGEO2526
- 676 Stothers, R.B. (2000). Climatic and demographic consequences of the massive volcanic eruption of 1258.  
677 *Climatic Change* 45, 361-374.
- 678 Svensson, A., Bigler, M., Blunier, T., Clausen, H. B., Dahl-Jensen, D., Fischer, H., Fujita, S., Goto-Azuma, K.,  
679 Johnsen, S. J., Kawamura, K., Kipfstuhl, S., Kohno, M., Parrenin, F., Popp, T., Rasmussen, S. O., Schwander, J.,  
680 Seierstad, I., Severi, M., Steffensen, J. P., Udisti, R., Uemura, R., Vallelonga, P., Vinther, B. M., Wegner, A.,  
681 Wilhelms, F., Winstrup, M. (2013). Direct linking of Greenland and Antarctic ice cores at the Toba eruption (74 ka  
682 BP). *Climate of the Past* 9, 749-766, <https://doi.org/10.5194/cp-9-749-2013>
- 683 Timmreck, C., Lorenz S.J., Crowley T.J., Kinne S., Raddatz T.J., Thomas M.A., Jungclaus J.H. (2009). Limited  
684 temperature response to the very large AD 1258 volcanic eruption. *Geophysical Research Letters* 36, L21708,  
685 doi:10.1029/2009GL040083
- 686 Vidal, C.M., Komorowski, J.-C., Metrich, N., Pratomo, I., Kartadinata, N., Prambada, O., Michel, A., Carazzo, G.,  
687 Lavigne, F., Rodysill, J., Fontijn, K., Surono, 2015. Dynamics of the major plinian eruption of Samalas in 1257 A.D.  
688 (Lombok, Indonesia). *Bulletin of Volcanology* 77, 73. <http://dx.doi.org/10.1007/s00445-015-0960-9>
- 689 Vidal, C.M., Metrich, N., Komorowski, J.-C., Indyo Pratomo, Michel, A., Kartadinata, N., Robert, V., Lavigne, F.  
690 (2016). The 1257 Samalas eruption (Lombok, Indonesia): the single greatest stratospheric gas release of the  
691 Common Era. *Scientific Reports* 6, Article number: 34868, DOI: 10.1038/srep34868
- 692 Wörner, G. (1999). Lithospheric dynamics and mantle sources of alkaline magmatism of the Cenozoic West  
693 Antarctic rift system. *Global and Planetary Change* 23, 61-77.

- 694 Yalcin, K., Wake, C.P., Kreutz, K.J., Germani, M.S., Whitlow, S.I. (2006). Ice core evidence for a second volcanic  
695 eruption around 1809 in the Northern Hemisphere. *Geophysical Research Letters* 33, L14706,  
696 doi:10.1029/2006GL026013
- 697 Young, C. L., Sokolik, I.N., Flanner, M.G., Dufek, J. (2014). Surface radiative impacts of ash deposits from the 2009  
698 eruption of Redoubt volcano, *Journal of Geophysical Research Atmosphere* 119, 11387–11397,  
699 doi:10.1002/2014JD021949
- 700 Zielinski, G.A. (1995). Stratospheric loading and optical depth estimates of explosive volcanism over the last  
701 2100 years derived from the GISP2 Greenland ice core. *Journal of Geophysical Research* 100, 20937-20955. DOI:  
702 10.1029/95JD01751
- 703 Zielinski, G.A., Dibb, J.E., Yang, Q., Mayewski, P.A., Whitlow, S., Twickler, M.S., Germani, M.S. (1997). Assessment  
704 of the record of the 1982 El Chichón eruption as preserved in Greenland snow. *Journal of Geophysical*  
705 *Research* 102 (D25), 30,031–30,045, doi:10.1029/97JD01574

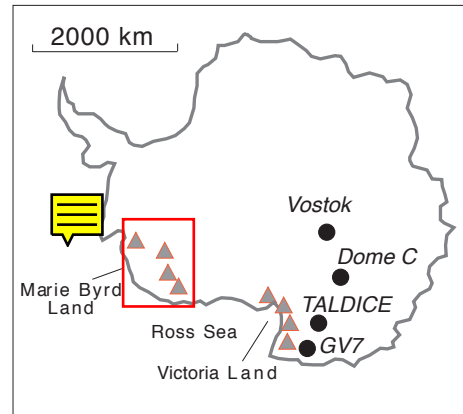
(a)

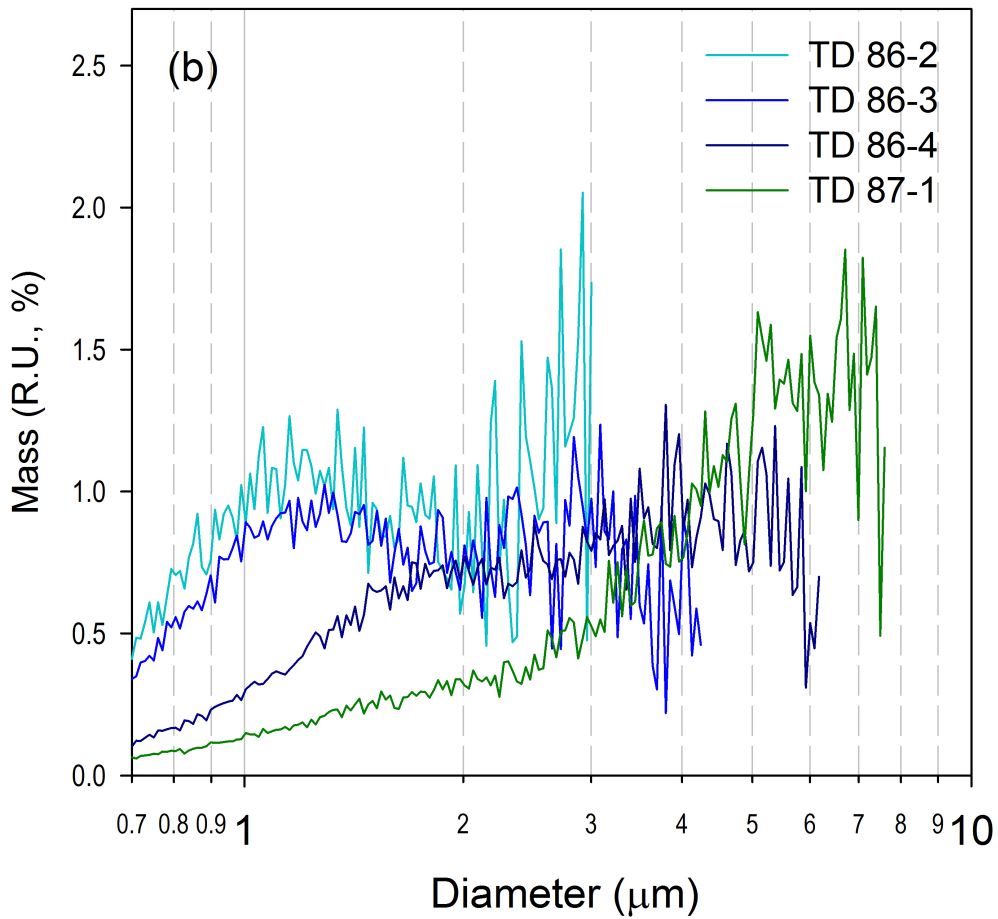
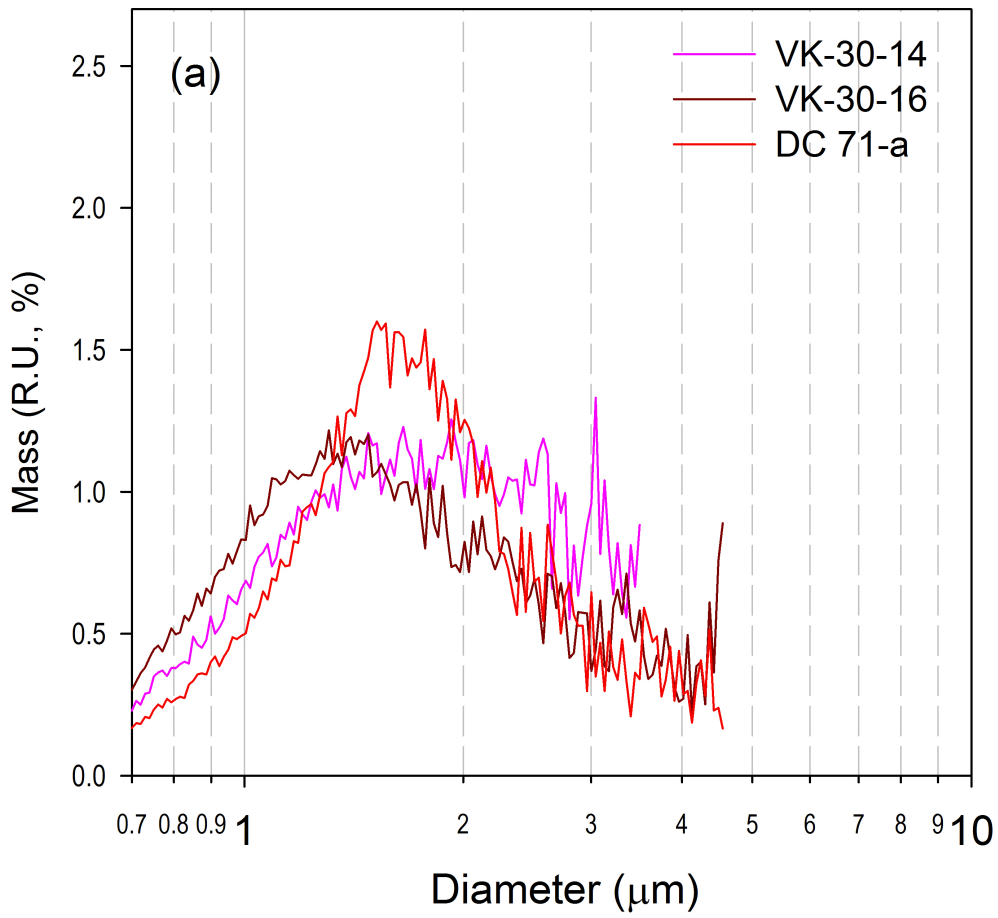
### Central Plateau

### Peripheral Plateau



(b)





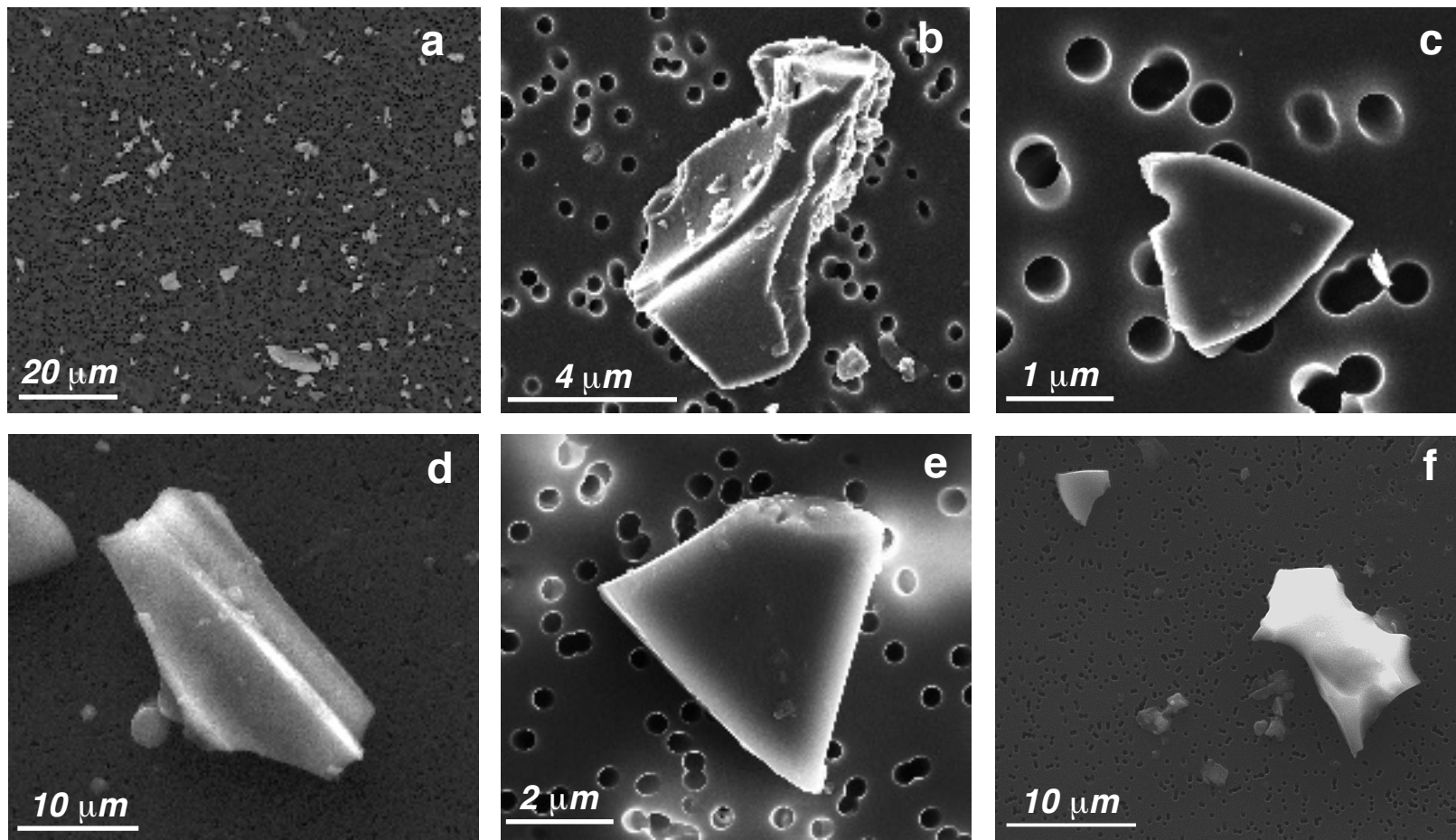
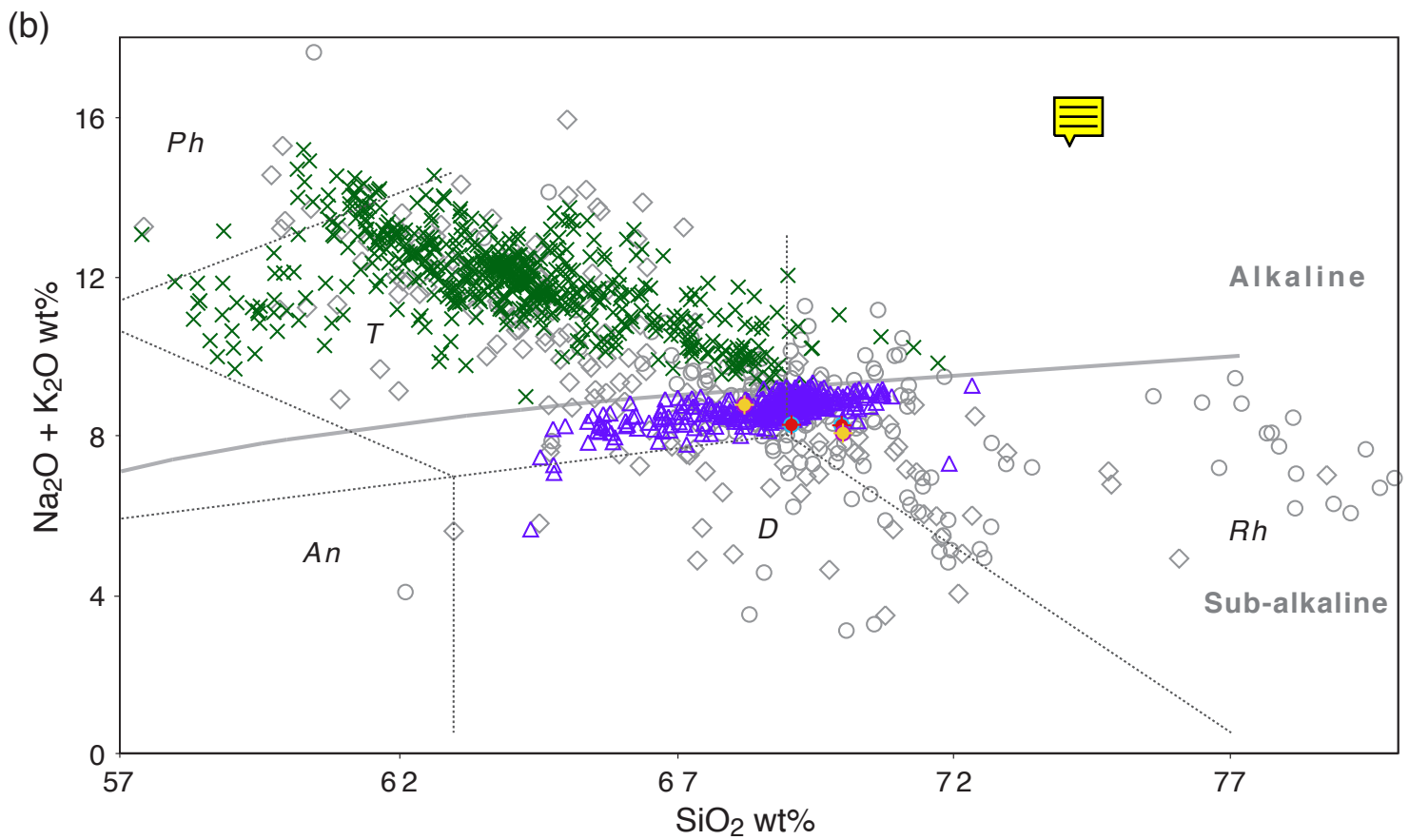
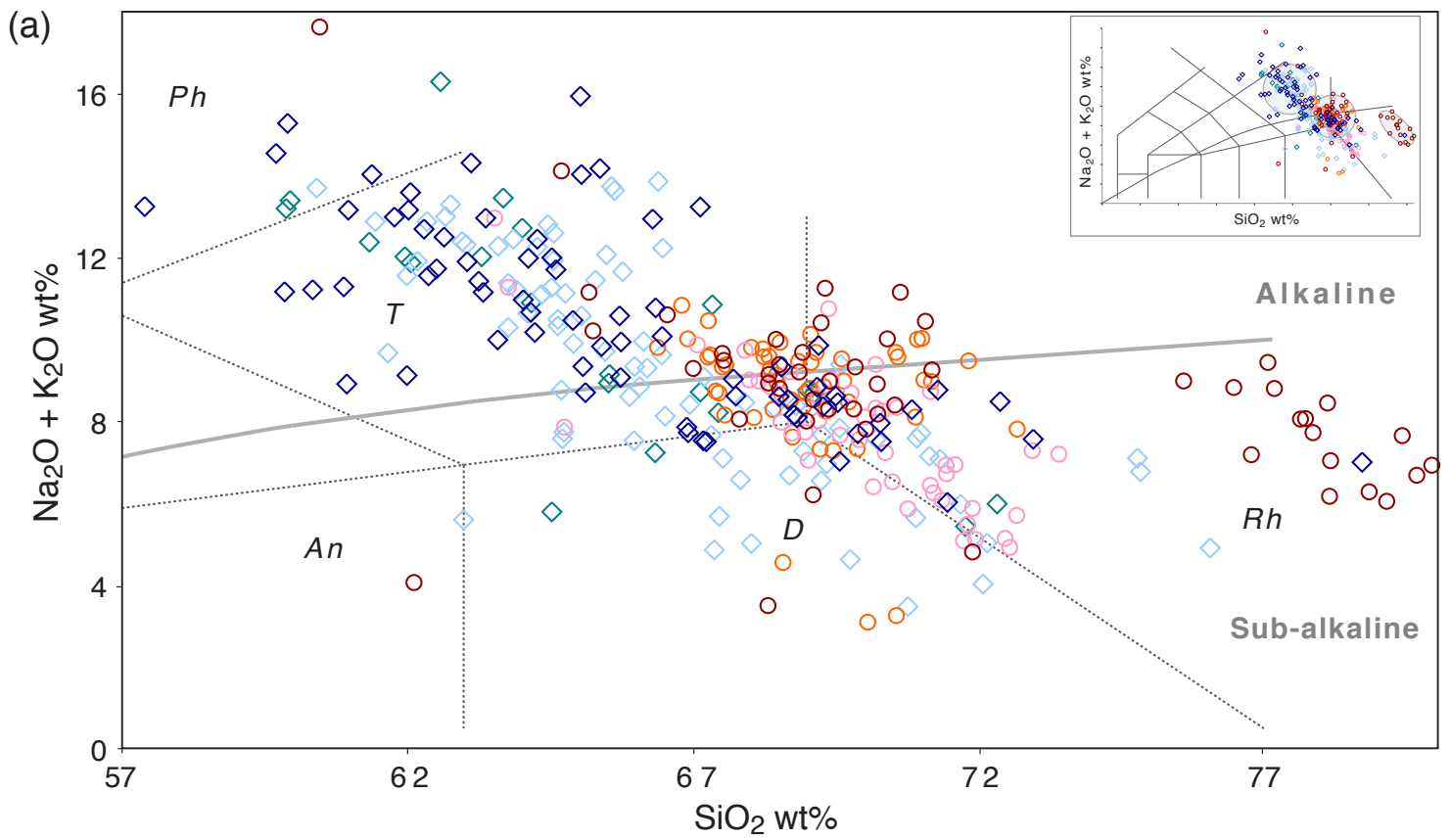
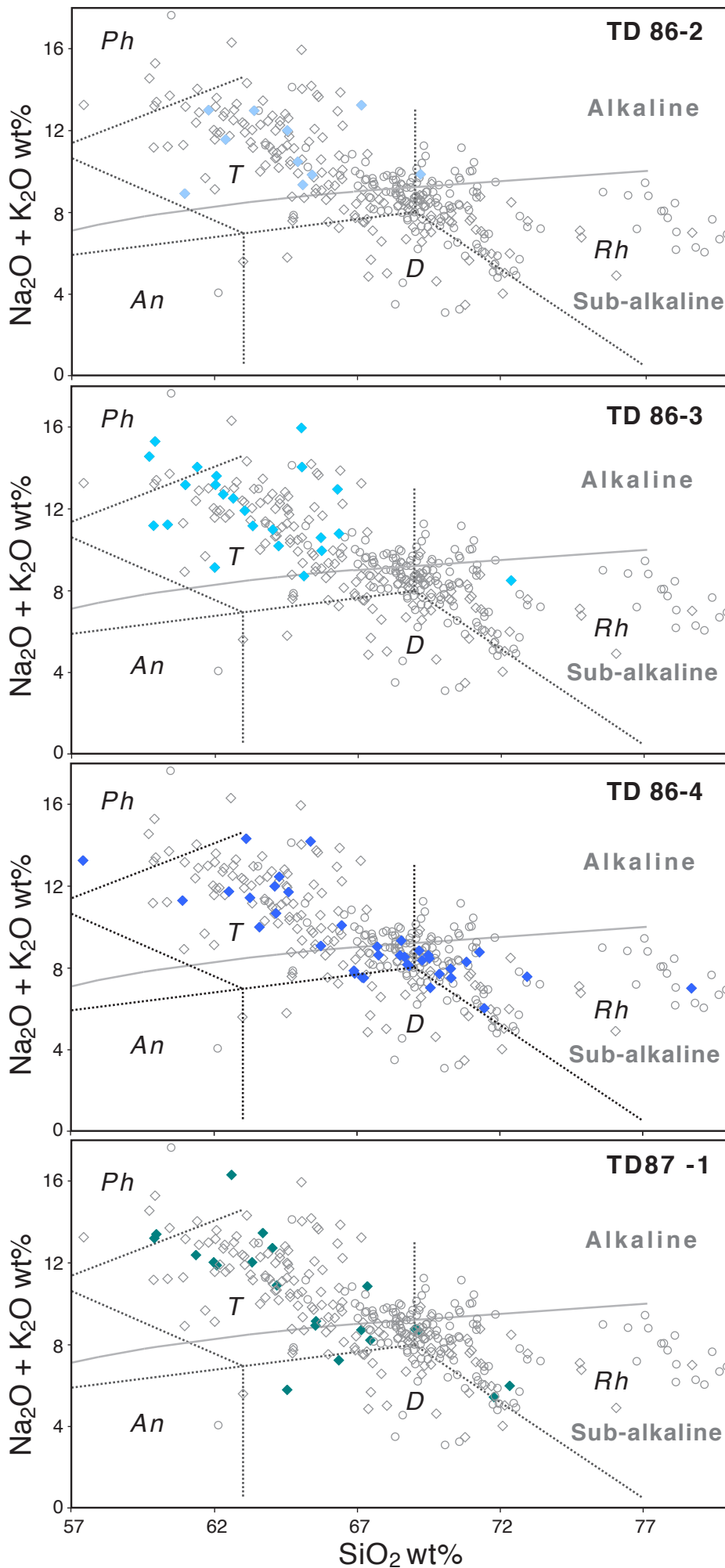


Fig. 3. Scanning electron microphotographs of volcanic glass particles from a, DC-71a; b-c, VK-14; d-e, TD87-1; f, TD86-4.





toward the upper part of the AD 1259 volcanic spike



1 Supplementary Material for

2

3 MULTIPLE SOURCES FOR TEPHRA FROM AD 1259 VOLCANIC SIGNAL IN ANTARCTIC ICE CORES

4

5 Biancamaria Narcisi<sup>1</sup>, Jean Robert Petit<sup>2</sup>, Barbara Delmonte<sup>3</sup>, Valentina Batanova<sup>4</sup>, Joël  
6 Savarino<sup>2</sup>

7

8 (1) ENEA, C.R. Casaccia, 00123 Roma, Italy, biancamaria.narcisi@enea.it

9

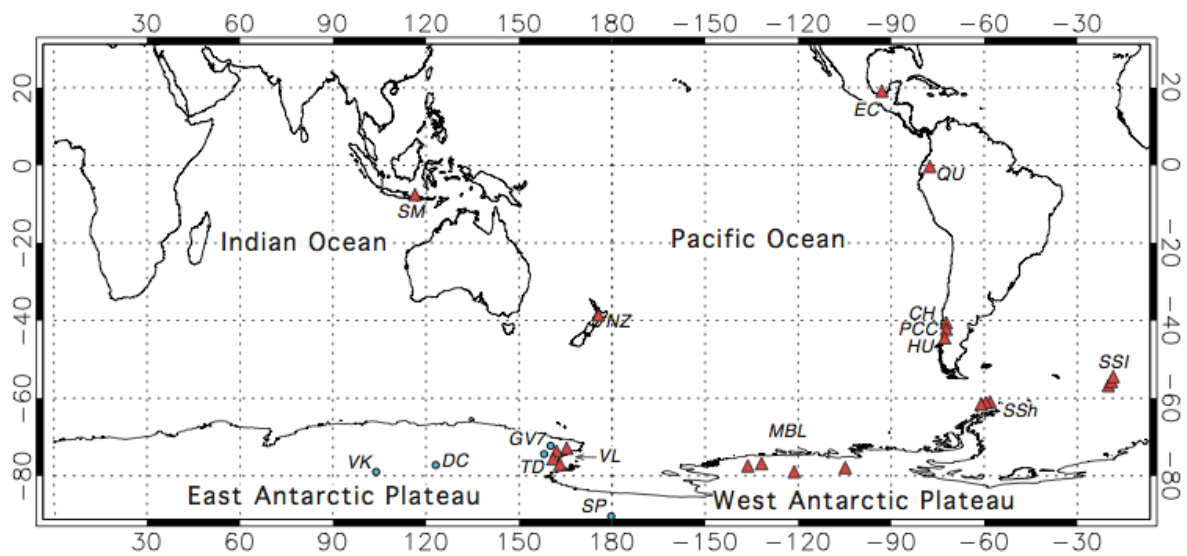
10 (2) Univ. Grenoble Alpes, CNRS, IRD, Grenoble INP, IGE, 38000 Grenoble, France

11 (3) Department of Earth and Environmental Sciences (DISAT), Univ. Milano-Bicocca, Piazza della Scienza, 20126  
12 Milano, Italy

13 (4) Univ. Grenoble Alpes, Univ. Savoie Mont Blanc, CNRS, IRD, IFSTTAR, ISTerre, 38000 Grenoble, France

Drilling Site/Ice core	Short name	Location, elevation a.s.l.	Accumulation rate (mm we year <sup>-1</sup> )	Drilling period	Reference	Present sample resolution (cm)
Concordia Station at Dome C	DC	75°06'S, 123°20'E, 3220 m	~25	2013-14	Schwander et al. (2001)	7
Vostok/BH6	VK	78°28'S, 106°48'E, 3488 m	~20	1991-92	Osipov et al. (2014)	5
Talos Dome/TALDICE	TD	72°49'S, 159°11'E, 2315 m	~80	2004-05	Severi et al. (2012)	5
GV7	GV7	70°41'S, 158°52'E, 1950 m	~240	2013-14	Frezzotti et al. (2007) Caiazzo et al. (2017)	15

14  
15 Table S1. Location and characteristics of the studied ice cores  
16  
17  
18



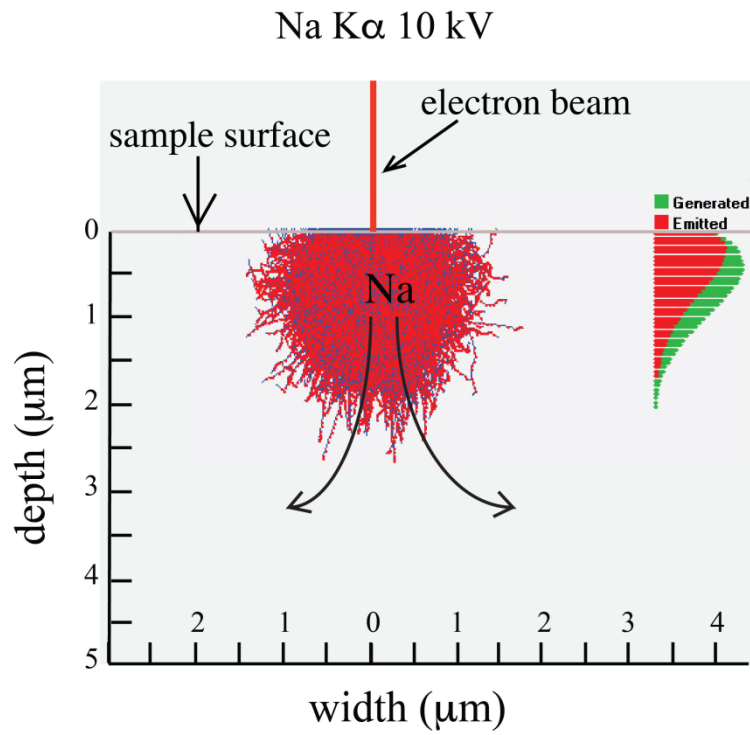
19  
20 Figure S1. World map showing the location of Antarctic ice core sites (blue dots) and of selected volcanic sources  
21 considered in the text (red triangles). Letters for sources are as follows. CH, Chaitén; EC, El Chichón; HU, Hudson;  
22 MBL, Marie Byrd Land; NZ, New Zealand; PCC, Puyehue-Cordon Caulle; QU, Quilotoa; SM, Samalas; SSh, South  
23 Shetland Islands; SSI, South Sandwich Islands; VL, Victoria Land

## 25 **Details of microprobe analysis**

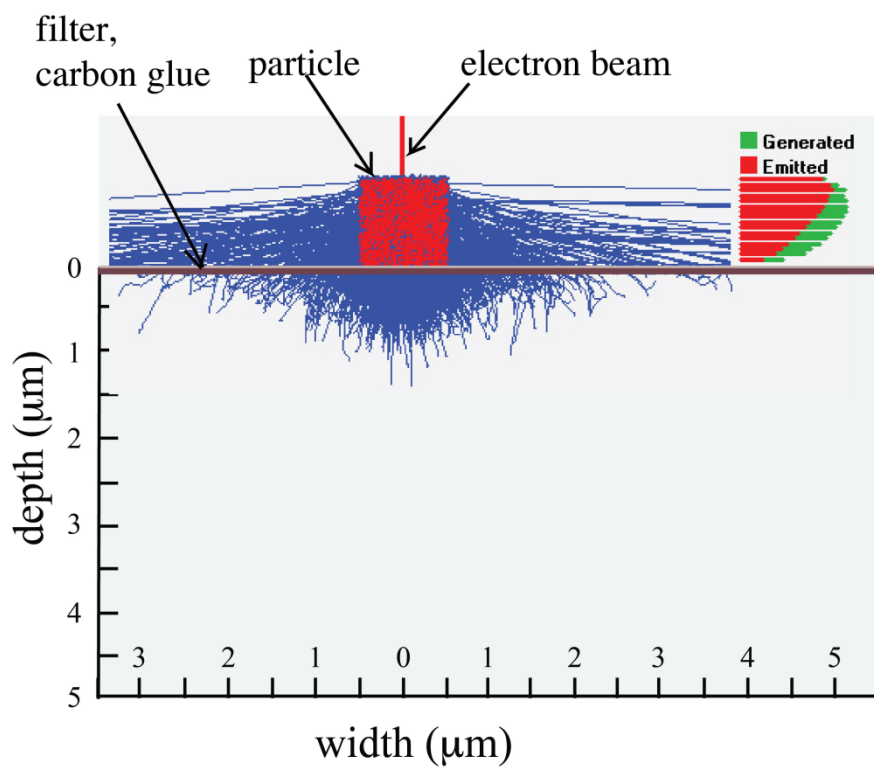
26

27 Although tephra embedding and polishing should be preferred for microprobe analysis, this was  
28 not possible here due to the small amount of material and its very fine grain size. Therefore,  
29 single-grain geochemical analysis was carried out on unpolished samples using a JEOL JXA-8230  
30 electron microprobe set up at the Institut des Sciences de Terre (ISTerre) of Grenoble. For  
31 analysis of small (1-3  $\mu\text{m}$ ) and thin (< 2  $\mu\text{m}$ ) unpolished tephra shards the analytical protocol  
32 with simultaneous WDS/EDS signal acquisition has been applied. We run Ti, Na, Mg, K, and Fe on  
33 WD spectrometers and Si, Ca, Al, on ED spectrometers. The following analytical conditions have  
34 been used: accelerating voltage 10kV, probe beam current 2 nA and beam diameter 1  $\mu\text{m}$ . The  
35 low accelerating voltage was selected to reduce X-ray excitation volume. Natural and synthetic  
36 minerals and glasses were used for standardisation: StHs6/80-G (Si, Al, Ca) and GOR132-G (Fe)  
37 synthetic glasses (Jochum et al, 2000 and GEOREM database), pure synthetic MgO (Mg),  
38 synthetic rutile (Ti), albite (Na), orthoclase (K). During analytical sessions the reference materials  
39 StHs6/80-G, ATHO-G (Jochum et al., 2000) and KE-12 (Metrich and Rutherford, 1992) ran as  
40 unknowns after each 40-50 analytical points to evaluate analytical accuracy and precision. Even  
41 at current as low as 2 nA the migration of sodium could be significant if the diameter of the  
42 electron beam is small (1  $\mu\text{m}$ ). The results of analysis of reference glasses and polished tephra  
43 samples analysed at traditional (Acc. voltage 15kV, probe current 5nA, beam diameter 5  $\mu\text{m}$ , e.g.  
44 Narcisi et al., 2016) and non-traditional (Acc. voltage 10kV, beam current 2nA, probe diameter 1  
45  $\mu\text{m}$ , this study) are in Table S2. We estimate that Na loss for polished samples analysed by 1  $\mu\text{m}$   
46 beam and non-traditional analytical conditions described above corresponds to 25% relative for  
47 samples with 4-7 wt% of  $\text{Na}_2\text{O}$  and 67-75 wt% of  $\text{SiO}_2$  (ATHO-G, KE-12, and samples RIN1392E  
48 and RIN1392A related to the AD 1257 Samalas medial tephra, Vidal et al., 2015) (Table S2). As it  
49 has been shown in several studies (e.g. Nielsen and Sigurdsson, 1981; Spray and Rae, 1995;  
50 Morgan and London, 1996) sodium migration from the excitation volume is a result of heating of  
51 the area of analysis by electron beam. According to Spray and Rae (1995) sodium migrates  
52 downward to space-charge layer within the sample. Figure S2 shows Monte Carlo electron  
53 trajectory simulation of the interaction volume as well as Na-K $\alpha$  generation and emission  
54 volumes for 10kV in common polished sample and unpolished 1x1  $\mu\text{m}$  particle on filter. These  
55 figures demonstrated how electron beam penetrates the samples of the different morphology.  
56 As follows from the modelling in case of analysis of small shards the Na migration does not take  
57 place because of small sample size. Analysis of small tephra shards often displayed low  
58 analytical total (30-60 %). Low and variable totals of analysis are result of small size of analytical  
59 area (smaller than excitation volume) (Figure S2-B). The analytical precision for the selected  
60 analytical conditions is in Table S2. While the analytical precision at 10 kV and 2 nA for the most  
61 analysed oxides is significantly lower than for traditional conditions it is still within reasonable  
62 error (5-15%).

A



B



63  
64  
65  
66  
67

Figure S2. Monte Carlo simulation of the interaction and emission volumes of X-rays at 10kV for Na-K $\alpha$  in Na-Si rich glass considered as A) common polished sample and B) small 1x1  $\mu\text{m}$  particle placed on the C-glue. The blue lines show the electron trajectory outside the particle.

Table S2. Composition of reference glasses and Samalas tephra samples measured at different analytical conditions

Sample	Reference	Analytical conditions	N	SiO <sub>2</sub>	TiO <sub>2</sub>	Al <sub>2</sub> O <sub>3</sub>	FeO <sub>tot</sub>	MnO	MgO	CaO	Na <sub>2</sub> O	K <sub>2</sub> O	Total
StHs6/80-G	this work	10kV, 2nA, 1 μm	15	63,56	0,69	17,61	4,46		1,95	5,38	4,33	1,29	99,28
±				0,45	0,10	0,33	0,26		0,11	0,33	0,30	0,04	
StHs6/80-G	this work	15kV, 5nA, 5 μm	15	63,73	0,69	17,86	4,29	0,08	1,94	5,26	4,62	1,28	99,75
±				0,21	0,01	0,18	0,08	0,03	0,04	0,06	0,12	0,03	
StHs6/80-G	Jochum et al. (2000) (a)			63,70	0,70	17,80	4,37	0,08	1,97	5,28	4,44	1,29	99,63
95%CL				0,50	0,02	0,20	0,07	0,00	0,04	0,09	0,14	0,02	
ATHO-G	this work	10kV, 2nA, 1 μm	12	75,64	0,26	11,95	3,14		0,09	1,72	2,79	2,61	98,20
±				0,59	0,04	0,21	0,27		0,03	0,25	0,47	0,08	
ATHO-G	this work	15kV, 5nA, 5 μm	12	75,88	0,24	12,30	3,14	0,11	0,09	1,71	3,98	2,64	100,08
±				0,32	0,02	0,21	0,06	0,03	0,01	0,03	0,10	0,04	
ATHO-G	Jochum et al. (2000) (a)			75,60	0,26	12,20	3,27	0,11	0,10	1,70	3,75	2,64	99,62
95%CL				0,70	0,02	0,20	0,10	0,01	0,01	0,03	0,31	0,09	
KE-12	this work	10kV, 2nA, 1 μm	12	71,56	0,32	7,92	8,93		0,01	0,39	5,36	4,09	98,60
±				0,45	0,08	0,20	0,45		0,02	0,20	0,23	0,09	
KE-12	this work	15kV, 5nA, 5 μm	12	71,01	0,30	7,84	8,30	0,26	0,03	0,37	7,01	4,23	99,35
±				0,33	0,01	0,11	0,08	0,03	0,02	0,01	0,17	0,04	
KE-12	Metrich and Rutherford (1992) (b)			70,30	0,33	7,60	8,36	0,26	nd	0,35	7,28	4,27	98,75
KE-12	Vidal et al. (2015) (c)		5	69,93	0,33	7,64	8,47	0,31	0,03	0,37	6,91	4,26	98,25
±				0,38	0,05	0,22	0,20	0,08	0,01	0,03	0,34	0,04	
RIN1392E	this work	10kV, 2nA, 1 μm	41	68,25	0,45	15,19	2,43		0,58	1,67	2,90	4,10	96,29
±				0,93	0,06	0,38	0,25		0,11	0,28	0,50	0,24	
RIN1392E	this work	15kV, 5nA, 5 μm	26	68,38	0,45	15,41	2,40	0,12	0,58	1,67	4,52	4,45	97,97
±				0,48	0,01	0,27	0,09	0,02	0,09	0,09	0,29	0,11	
RIN1392E	Vidal et al. (2015) (c)		10	70,09	0,47	15,65	2,51	0,14	0,60	1,80	3,52	4,39	99,17
±				0,69	0,07	0,28	0,10	0,07	0,05	0,21	0,47	0,22	
RIN1392A	this work	10kV, 2nA, 1 μm	48	67,95	0,45	16,05	2,81		0,74	2,22	3,59	3,99	98,68
±				0,65	0,07	0,26	0,22		0,07	0,25	0,35	0,10	
RIN1392A	this work	15kV, 5nA, 5 μm	48	67,67	0,45	16,16	2,66	0,12	0,72	2,18	4,73	4,11	98,81
±				0,49	0,02	0,21	0,07	0,02	0,02	0,05	0,19	0,06	
RIN1392A	Vidal et al. (2015) (c)		16	68,24	0,46	16,11	2,70	0,11	0,73	2,22	4,69	4,16	99,42
±				0,77	0,07	0,31	0,12	0,05	0,04	0,13	0,19	0,11	



Notes: Oxides reported in wt%. N - number of analyses. Reproducibility (±) is shown as 1 standard deviation of average.

(a) reference values; (b) whole rock data; (c) EPMA data.


68  
69  
70  
71  
72

Table S2. Composition of reference glasses and Samalas tephra samples measured at different analytical conditions.

73 **Potential sources for the ice-core dacitic glass population**

74  
75 Our attempt  source identification was based upon comparison with bibliographic information  
76 for volcanoes that have been active during post-glacial times. We considered as constraining  
77 features the chronostratigraphy of the deposits, the character of volcanic activity and the  
78 chemical signature of the material. However, a matching source depends on the data available  
79 in the literature. Inaccessible volcanoes may be  ~~provided with~~ stratigraphic records that are still  
80 incomplete or poorly age constrained. The possibility that our tephra may represent a hitherto  
81 unknown eruption in the proximal sequence cannot be entirely excluded. As for chemical  
82 features of deposits from proximal contexts, in order to avoid misleading correlations we took  
83 into account only sources for which single-shard microprobe data are available. We consider in  
84 fact bulk-rock analyses of near-vent samples, often affected by the presence of minerals on  
85 xenoliths, unsuitable for comparison with the present shard-specific dataset. However, we are  
86 aware that proximal and distal tephra components of the same eruption may have slightly  
87 different compositions and this may represent a further problem of our approach. On the other  
88 hand, here we considered a large set of possible volcanic sources within and surrounding the  
89 Antarctic continent, more extended than that employed in previous studies. This strategy,  
90 requiring scrutiny of a high number of relevant published papers, allowed us to confidently rule  
91 out clearly dissimilar sources and to ascribe the investigated ice-core tephra to the parent  
92 eruption.

93  
94 Figure S1 illustrates location of a few volcanoes considered in this discussion. Graphical  
95 comparison of the composition of individual ice-core shards with glass analyses from proximal  
96 source deposits (Figure S3) supports the following considerations.

97 Regardless of age of proximal activity, we could readily exclude volcanism of South Sandwich  
98 Islands (SSI) in the Southern Atlantic Ocean, producing several tephra preserved in Central EAP  
99 (e.g., Narcisi et al., 2010, and references therein), because of its low-K tholeiitic nature (e.g.,  
100 Nielsen et al., 2007), as well as volcanoes in the South Shetland Islands (Antarctic Peninsula  
101 region) that display predominantly basaltic and basaltic  andesitic compositions (Kraus et al.,  
102 2013; Antoniadou et al., 2018). Both provinces are clearly dissimilar in composition with the ice-  
103 core glass.

104 Careful attention was paid to post-glacial volcanoes of the Andean belt representing very  
105 efficient producers of sub-alkaline (calc-alkaline) tephra. These could be eligible candidates  
106 considering that the westerly atmospheric circulation penetrating the EAP favours the rapid  
107 transport and deposition of dust and tephra from South America to Antarctica (e.g., Pitts and  
108 Thomason, 1993; Delmonte et al., 2008; Narcisi et al., 2012; Koffman et al., 2017). On the basis of  
109 numerous studies over the last decades, the eruptive chronologies of many of these volcanic  
110 centres are well constrained, thus helping us to rule out a number of them.

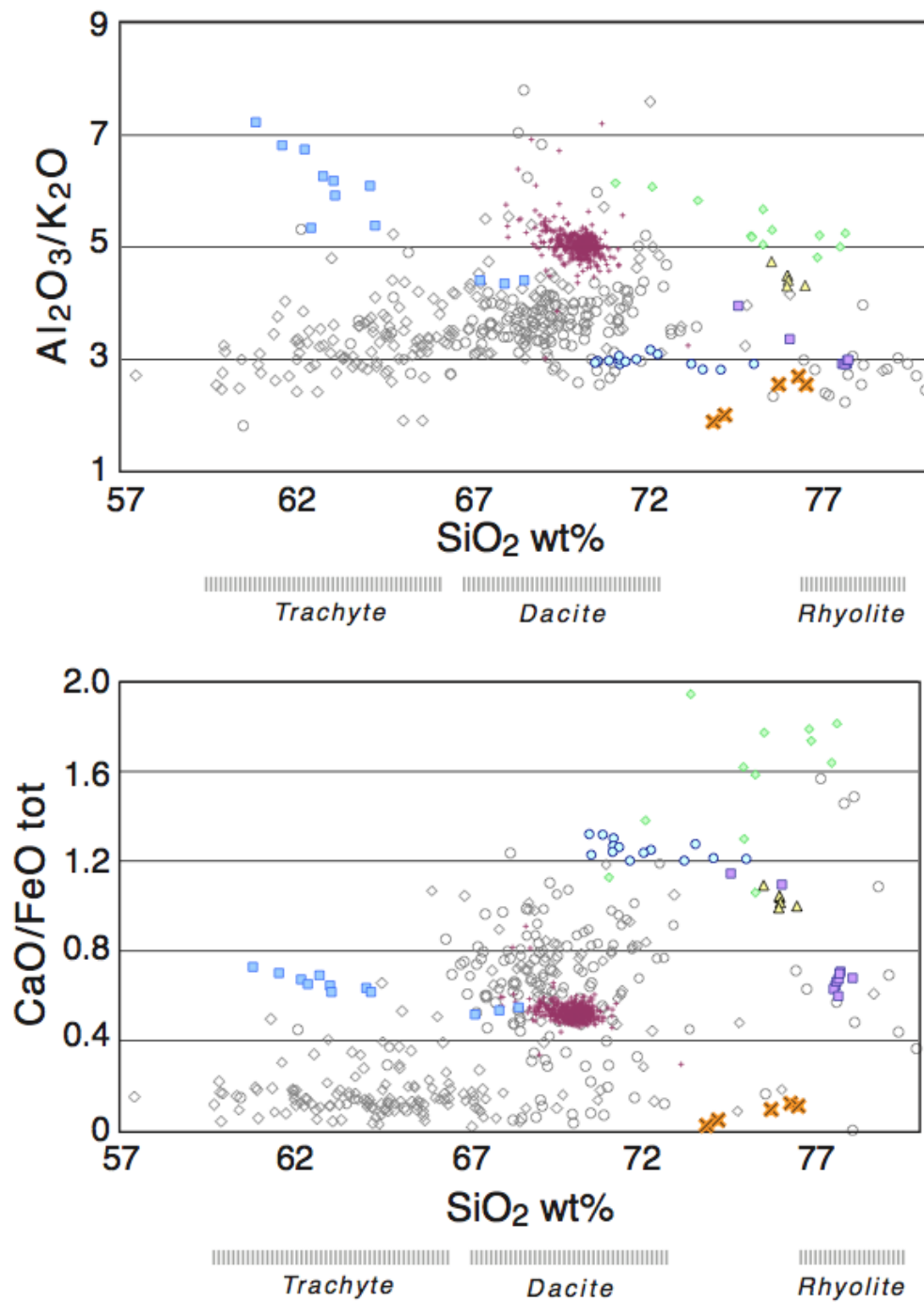
111 In particular, in the Southern and Austral Volcanic Zones of the Andes (latitudes between 33 to  
112 55°S) about 20 volcanoes produced explosive eruptions with significant regional or even  
113 hemispheric impact (Fontijn et al., 2014). However, the largest Holocene explosive eruptions of  
114 volcanoes in the southernmost Andes producing regionally widespread tephra layers are dated  
115 back at least to 3 ka (Stern, 2008) and so are too old to be related with the studied tephra. Other  
116 volcanoes of the Southern Volcanic Zone that either are too old or do not show geological



117 evidence of energetic explosive activity in mid-13<sup>th</sup> century to be considered as likely sources are  
118 Calbuco (41°33'S, Watts et al., 2011), Mocho-Choshuenco (39°55'S, Rawson et al., 2015),  
119 Quetrupillán (39°30' S, Fontjin et al., 2016), Sollipulli (38°58'S; Naranjo et al., 1993), Lonquimay  
120 (38°22'S, Gilbert et al., 2014), Quizapu–Cerro Azul (35°39'S, Ruprecht et al., 2012) San Pedro  
121 (36°S, Singer et al., 1997). Similarly, we can exclude volcanoes of the Central Volcanic Zone of  
122 the Andes (latitudes between 14° and 29°S) characterised by high-K calc-alkaline compositions.  
123 Here, the two last major explosive events were the 2-ka BP plinian eruption of El Misti volcano  
124 (Thouret et al., 2001) and the AD 1600 eruption of Huaynaputina volcano (e.g., Lavallée et al.,  
125 2006), both inconsistent with age of the ice tephra sample. The remaining explosive activity was  
126 small to moderate, so most likely not capable of dispersing ash onto the Antarctic ice sheet.  
127 Farther north, also at the Andean volcanoes of Chimborazo (1°28'S, Barba et al., 2008) and  
128 Cotopaxi (0°38'S, Hall and Mothes, 2008) the recorded activity is not appropriate as either age or  
129 character to suggest a linkage with our tephra. In the Northern Hemisphere, according to marine  
130 tephrostratigraphy offshore the southern Central American Volcanic Arc (7-9 °N) documenting  
131 explosive activity of Costa Rica and Nicaragua volcanoes, the most recent marker is 3.5 ka old  
132 (Schindlbeck et al., 2016), thus much older than our ice-core tephra. Terrestrial  
133 volcanostratigraphies of Irazú (9°58'N, Benjamin et al., 2007), Apoyeque (12°14'N, Kutterolf et al.,  
134 2011) and Ilopango (13°67'N, Mehringer et al., 2005) do not show any suitable tephra deposit of  
135 appropriate age. The voluminous eruption of El Metate (19°32'N, Mexico) dated at ~ AD 1250 was  
136 purely effusive (Chevrel et al., 2015), making it an unlikely candidate.

137 We carried out a comparison between our glass-shard microprobe data and the composition of  
138 selected calc-alkaline tephra sources active in the last millennium (Figure S3). In particular, we  
139 considered recent explosive products of the American volcanoes of Chaitén (42°49'S, Moreno et  
140 al., 2015), Puyehue-Cordon Caulle (40°59'S, Mil Hojas tephra, modelled age  $0.84 \pm 0.18$  cal ka BP,  
141 Fontjin et al., 2016), Hudson (45°54'S, Kratzmann et al., 2009), Quilotoa (~ AD 1280, 0°51'S,  
142 Stewart and Castro, 2016), El Chichón (6<sup>th</sup>-century deposits, 17°22'N, Nooren et al., 2017) along  
143 with tephra erupted during the Kaharoa eruption in New Zealand (AD  $1314 \pm 12$ ; e.g., Nairn et al.,  
144 2004) and from Marie Byrd Land volcanoes found in the marine realm (Shane and Froggatt,  
145 1992). It can be seen that none of these satisfactorily fit the dacitic chemistry of the ice-core  
146 tephra component and consequently cannot be likely counterparts. Note that El Chichón  
147 volcano was previously suggested as a probable source for the polar tephra in the South Pole  
148 (SP) and Greenland ice cores (Palais et al., 1992). Although the El Chichón historic volcanic  
149 record does not preclude this possibility (Espíndola et al., 2000), the present comparison  
150 highlights appreciable compositional differences between the studied dacitic tephra and the  
151 proximal volcanic deposits, thus excluding the former attribution.

152  
153 We finally found a positive chemical match between dacitic glass shards trapped within ice and  
154 products of AD 1257 Samalas volcanic eruption, the cataclysmic event that occurred in the  
155 Indonesian Archipelago (8°33'S) and ranking among the greatest volcanic events of the  
156 Holocene (e.g., Lavigne et al., 2013; Vidal et al., 2015, 2016; Alloway et al., 2017) (Figure 4b, main  
157 text). Note that our chemical results are also consistent with microprobe data of Samalas samples  
158 analysed within this work (Table S2).



159  
 160 Figure S3. Major element biplots for the analysed ice-core shards (in grey-scale) compared with glass geochemical  
 161 analyses for selected potential sources and counterparts (data from Moreno et al., 2015; Fontijn et al., 2016; Nairn et  
 162 al., 2004; Kratzmann et al., 2009; Nooren et al., 2017; Stewart and Castro, 2016; Shane and Froggatt, 1992). Location  
 163 of considered source volcanoes is shown in Supplementary Figure S1.

Table S3. Representative major element composition of individual glass shards determined by electron microprobe analysis. Values are given in weight % oxide and are normalised to 100%. Total iron is expressed as FeO. MnO not determined. Glass populations as defined in the main text

Analytical session	DC 71-a	SiO <sub>2</sub>	TiO <sub>2</sub>	Al <sub>2</sub> O <sub>3</sub>	FeO <sub>tot</sub>	MgO	CaO	Na <sub>2</sub> O	K <sub>2</sub> O	Original Total	Glass pop.
<b>May 2015</b>											
	1259_1-p3	67.57	0.60	15.68	4.41	0.94	2.65	4.24	3.91	60.66	diacitic
	1259_1-p6	67.27	0.56	15.31	4.33	0.68	2.27	5.16	4.42	64.67	diacitic
	1259_1-p10	69.07	0.37	15.87	2.05	0.82	1.71	5.41	4.71	77.56	diacitic
	1259_1-p14	68.86	0.55	15.72	2.82	0.68	1.90	4.75	4.71	67.51	diacitic
	1259_1-p16	68.37	0.47	15.52	3.22	0.98	2.13	4.68	4.62	67.66	diacitic
<b>December 2015</b>											
	1259_p6	69.33	0.51	15.68	3.44	0.77	2.02	4.44	3.81	77.58	diacitic
	1259_p13	67.32	0.59	15.59	3.29	0.90	2.69	5.21	4.41	72.66	diacitic
	1259_p16	70.90	0.44	15.43	2.81	0.76	1.56	3.67	4.43	90.67	diacitic
	1259_p19	68.41	0.62	16.05	3.44	0.94	2.25	4.19	4.09	72.85	diacitic
	1259_p20	67.47	0.53	16.78	3.17	0.84	2.52	4.69	4.01	91.60	diacitic
	1259_p31	69.65	0.52	15.56	3.16	0.60	1.54	4.25	4.75	71.40	diacitic
	1259_p40	68.47	0.51	14.76	3.78	1.05	2.29	4.65	4.49	61.73	diacitic
	1259_p42	69.05	0.39	15.07	3.64	0.89	2.16	4.68	4.12	67.41	diacitic
	1259_p44	69.61	0.49	15.83	2.08	0.85	1.61	4.92	4.61	66.34	diacitic
<b>Analytical session VK -14</b>											
<b>October 2016</b>											
	BH6-30-14_p7	69.38	0.50	15.05	2.62	0.59	1.10	5.51	5.25	76.31	diacitic
	BH6-30-14_p8	70.33	0.43	15.96	2.56	0.65	1.81	4.04	4.22	90.59	diacitic
	BH6-30-14_p17	68.72	0.44	15.61	2.80	0.73	2.43	4.06	4.24	77.77	diacitic
	BH6-30-14_p26	67.09	0.60	15.33	3.65	0.95	2.51	4.91	4.96	79.05	diacitic
	BH6-30-14_p27	68.17	0.50	16.29	2.89	0.86	2.31	4.97	4.01	95.16	diacitic
	BH6-30-14_p50	69.78	0.66	16.13	2.46	0.70	1.57	4.36	4.33	95.08	diacitic
	BH6-30-14_p75	69.21	0.53	16.56	2.96	0.71	2.02	4.02	4.00	93.55	diacitic
	BH6-30-14_p89	63.54	0.47	16.04	6.18	0.09	0.72	8.07	4.69	96.72	trachytic
	BH6-30-14_p90	63.78	0.48	17.30	6.17	0.14	0.86	6.59	4.69	91.31	trachytic
	BH6-30-14_p91	68.00	0.63	15.48	3.50	0.73	2.34	4.83	4.18	68.01	diacitic
	BH6-30-14_p92	67.92	0.55	15.67	3.21	0.89	2.02	5.13	4.61	84.58	diacitic
	BH6-30-14_p110	71.16	0.41	16.44	1.40	0.48	1.37	4.29	4.44	96.57	diacitic
	BH6-30-14_p120	70.58	0.49	16.17	2.00	0.79	1.64	4.32	4.02	97.06	diacitic
	BH6-30-14_p146	68.56	0.56	16.12	2.79	1.15	2.17	4.46	4.19	90.30	diacitic
	BH6-30-14_p153	69.21	0.45	16.04	2.54	0.65	2.50	4.54	4.07	87.56	diacitic
<b>Analytical session VK -16</b>											
<b>October 2016</b>											
	BH6-30-16_p10	69.40	0.50	16.29	2.37	0.75	1.70	4.88	4.11	68.11	diacitic
	BH6-30-16_p22	78.15	0.00	13.81	0.63	0.30	0.94	2.70	3.48	90.33	ryholitic
	BH6-30-16_p29	69.38	0.43	16.10	2.46	0.60	2.72	4.25	4.06	76.28	diacitic
	BH6-30-16_p63	77.19	0.18	12.70	0.43	0.02	0.68	3.43	5.38	69.81	ryholitic
	BH6-30-16_p68	77.07	0.19	12.36	0.26	0.13	0.55	4.30	5.15	82.58	ryholitic
	BH6-30-16_p76	68.53	0.48	15.22	3.64	0.91	1.82	5.21	4.19	68.17	diacitic
	BH6-30-16_p77	68.86	0.50	16.19	3.50	0.66	1.08	5.05	4.16	82.05	diacitic
	BH6-30-16_p82	68.34	0.62	16.28	3.11	0.82	1.48	4.62	4.52	71.97	diacitic
	BH6-30-16_p83	65.26	0.39	14.21	8.55	0.62	0.76	5.04	5.17	63.35	trachytic
	BH6-30-16_p87	70.24	0.47	15.16	2.98	0.67	1.57	4.59	4.32	70.77	diacitic
	BH6-30-16_p91	69.11	0.42	16.28	2.99	0.75	1.92	4.51	4.02	89.56	diacitic
	BH6-30-16_p95	67.53	0.42	15.97	2.78	0.76	2.78	5.27	4.39	76.03	diacitic
	BH6-30-16_p99	68.93	0.54	15.49	3.49	0.67	1.20	5.03	4.65	63.47	diacitic
	BH6-30-16_p117	69.85	0.59	15.54	3.09	0.54	1.07	4.53	4.79	60.37	diacitic
	BH6-30-16_p130	77.72	0.62	12.77	0.37	0.00	0.21	3.36	4.59	69.69	ryholitic
	BH6-30-16_p134	67.55	0.61	15.51	3.85	0.70	2.28	5.23	4.26	73.56	diacitic
	BH6-30-16_p140	77.64	0.19	12.44	0.98	0.13	0.56	2.50	5.55	88.98	ryholitic
	BH6-30-16_p160	68.33	0.40	15.91	3.45	0.84	2.14	4.78	4.15	79.73	diacitic
<b>Analytical session TD 87-1</b>											
<b>December 2015</b>											
	87-1-p27	63.69	0.24	17.06	4.07	0.06	1.42	7.63	5.82	90.22	trachytic
	87-1-p37	64.03	0.34	16.21	5.08	0.20	1.41	6.98	5.75	94.01	trachytic
	87-1-p42	62.06	0.49	16.03	7.97	0.12	1.43	6.74	5.14	68.65	trachytic
	87-1-p45	61.97	0.44	16.46	7.54	0.19	1.37	7.09	4.94	89.66	trachytic
	87-1-p47	61.35	0.61	15.99	6.23	0.34	3.09	7.75	4.63	95.15	trachytic
	87-1-p50	63.32	0.43	16.57	6.80	0.07	0.79	6.52	5.00	91.36	trachytic
<b>Analytical session TD 86-4</b>											
<b>December 2015</b>											
	86-4A-14	69.18	0.46	15.67	2.75	0.89	2.20	4.56	4.28	86.15	diacitic
	86-4A-15	78.72	0.53	12.22	0.93	0.04	0.57	2.83	4.37	90.99	ryholitic
	86-4A-30	69.51	0.45	16.07	2.57	0.58	2.14	4.25	4.37	92.92	diacitic
	86-4A-34	68.83	0.48	16.33	3.31	0.75	2.20	4.11	3.96	89.23	diacitic
	86-4A-38	64.29	0.53	14.92	7.44	0.13	0.24	7.26	5.19	79.68	trachytic
	86-4A-51	68.56	0.49	15.70	2.97	0.76	2.18	4.75	4.59	83.72	diacitic
	86-4A-60	63.26	0.45	15.88	7.63	0.13	1.23	6.26	5.16	77.80	trachytic
	86-4A-61	62.52	0.43	15.99	8.23	0.12	0.98	6.23	5.90	71.52	trachytic
	86-4A-65	69.54	0.46	15.69	2.89	0.75	2.21	4.27	4.19	92.31	diacitic
	86-4A-66	64.18	0.41	16.36	7.36	0.14	0.88	6.09	4.57	85.33	trachytic
	86-4A-67	68.78	0.62	16.94	2.35	0.85	2.32	4.06	4.10	88.71	diacitic
	86-4A-89	64.13	0.41	16.37	6.20	0.10	0.80	6.76	5.23	75.48	trachytic
	86-4A-90	64.61	0.44	15.50	6.93	0.17	0.65	6.18	5.53	83.29	trachytic
	86-4A-99	69.29	0.43	16.23	3.18	0.68	1.82	4.03	4.34	88.59	diacitic
<b>Analytical session TD 86-3</b>											
<b>December 2015</b>											
	86-3a-25	62.66	0.27	16.70	7.11	0.12	0.64	7.32	5.18	95.57	trachytic
	86-3a-27	62.04	0.33	16.28	7.05	0.16	0.98	8.31	4.85	91.91	trachytic
	86-3a-30	62.07	0.36	16.37	6.76	0.08	0.76	8.60	5.00	86.71	trachytic
	86-3a-38	61.39	0.57	13.81	8.41	0.20	1.58	8.77	5.26	89.03	trachytic
	86-3a-66	63.06	0.37	16.00	7.78	0.03	0.86	7.48	4.42	67.57	trachytic
	86-3a-72	62.31	0.50	16.07	7.53	0.06	0.83	7.83	4.87	81.82	trachytic
	86-3a-76	64.04	0.34	16.86	6.72	0.14	0.92	6.14	4.17	92.14	trachytic
<b>Analytical session TD 86-2</b>											
<b>December 2015</b>											
	86-2A-7	61.79	0.47	15.64	8.34	0.14	0.63	7.21	5.79	63.85	trachytic
	86-2A-12	64.54	0.41	16.68	5.52	0.19	0.65	7.18	4.82	95.52	trachytic
	86-2A-13	69.21	0.68	15.23	3.06	0.77	1.20	5.32	4.54	62.11	diacitic
	86-2A-14	65.09	0.43	17.62	6.62	0.05	0.85	5.32	4.02	96.45	trachytic
	86-2A-20	63.38	0.45	16.38	6.58	0.08	0.29	7.58	5.29	91.48	trachytic
<b>Analytical session GV7 295-1</b>											
<b>February 2016</b>											
	295-1-p12	68.43	0.45	16.67	3.05	0.86	2.20	4.43	3.91	98.29	diacitic
	295-1-p24	64.92	0.46	17.70	6.21	0.07	0.73	5.40	4.50	100.14	trachytic
<b>June 2016</b>											
	295-1-p27	62.78	0.48	16.50	6.18	0.11	0.64	8.21	5.08	91.29	trachytic
	295-1-p31	65.06	0.22	17.98	4.77	0.00	1.39	5.46	5.12	68.02	trachytic
	295-1-p56	64.57	0.11	16.83	5.50	0.07	1.00	7.01	4.92	89.80	trachytic
	295-1-p66	66.40	0.41	16.68	2.10	0.00	0.54	7.75	6.11	97.83	trachytic
	295-1-p67	70.93	0.59	15.66	2.95	0.68	1.61	3.38	4.21	88.51	diacitic
<b>Analytical session GV7 294-4</b>											
<b>February 2016</b>											
	294-4-p2	63.78	0.38	16.40	7.22	0.19	1.72	5.75	4.55	83.47	trachytic
	294-4-p3	61.46	0.36	16.52	8.11	0.02	0.66	8.49	4.39	93.16	trachytic
	294-4-p10	67.92	0.48	16.29	3.15	0.87	2.82	4.34	4.12	92.97	diacitic
	294-4-p14	60.43	0.35	15.66	8.91	0.14	0				

168 **References for Supplementary Material**

169

170 Alloway, B.V., Supriyati Andreastuti, Ruly Setiawan, John Miksic, Quan Hua (2017). Archaeological implications of a  
171 widespread 13th Century tephra marker across the central Indonesian Archipelago. *Quaternary Science Reviews*  
172 155, 86-99. <https://doi.org/10.1016/j.quascirev.2016.11.020>

173 Antoniades, D., Giralt, S., Geyer, A., Álvarez-Valero, A.M., Pla-Rabes, S., Granados, I., Liu, E.J., Toro, M., Smellie, J.L.,  
174 Oliva, M. (2018). The timing and widespread effects of the largest Holocene volcanic eruption in Antarctica.  
175 *Scientific Reports* 8, 1–11, DOI:10.1038/s41598-018-35460-x

176 Barba, D., Robin, C., Samaniego, P., Eissen, J.-P. (2008). Holocene recurrent explosive activity at Chimborazo  
177 volcano (Ecuador). *Journal of Volcanology and Geothermal Research* 176 (1), 27-35,  
178 <https://doi.org/10.1016/j.jvolgeores.2008.05.004>

179 Benjamin, E.R., Plank, T., Wade, J.A., Kelley, K.A., Hauri, E.H., Alvarado, G.E. (2007). High water contents in basaltic  
180 magmas from Irazú Volcano, Costa Rica. *Journal of Volcanology and Geothermal Research* 168, 68–92,  
181 <https://doi.org/10.1016/j.jvolgeores.2007.08.008>

182 Caiazza, L., Baccolo, G., Barbante, C., Becagli, S., Bertò, M., Ciardini, V., Crotti, I., Delmonte, B., Dreossi, G., Frezzotti,  
183 M. et al. (2017). Prominent features in isotopic, chemical and dust stratigraphies from coastal East Antarctic ice  
184 sheet (Eastern Wilkes Land). *Chemosphere* 176, 273-287, <https://doi.org/10.1016/j.chemosphere.2017.02.115>

185 Chevrel, M., Siebe, C. Guilbaud, M.N. Salinas, S. (2015). The AD 1250 El Metate shield volcano (Michoacán): Mexico's  
186 most voluminous Holocene eruption and its significance for archaeology and hazards. *The Holocene* 26, 471-488,  
187 DOI: 10.1177/0959683615609757

188 Delmonte, B., Andersson, P.S., Hansson, M., Schöberg, H., Petit, J.R., Basile-Doelsch, I., Maggi, V. (2008). Aeolian dust  
189 in East Antarctica (EPICA-Dome C and Vostok): Provenance during glacial ages over the last 800 kyr. *Geophysical*  
190 *Research Letters* 35 L07703, doi:10.1029/2008GL033382

191 Espíndola, J.M., Macías, J.L., Tilling, R.I., Sheridan M.F. (2000). Volcanic history of El Chichón Volcano (Chiapas,  
192 Mexico) during the Holocene, and its impact on human activity. *Bulletin of Volcanology* 62, 90-104.

193 Fontijn, K., Lachowycz, S.M., Rawson, H., Pyle, D.M., Mather, T.A., Naranjo, J.A., Moreno- Roa, H. (2014). Late  
194 Quaternary tephrostratigraphy of southern Chile and Argentina. *Quaternary Science Reviews* 89, 70–84.

195 Fontijn, K., Rawson, H., Van Daele, M., Moernaut, J., Abarzúa, A.M., Heirman, K., Bertrand, S., Pyle, D.M. et al. (2016).  
196 Synchronisation of sedimentary records using tephra: A postglacial tephrochronological model for the Chilean Lake  
197 District. *Quaternary Science Reviews* 137, 234-254, <https://doi.org/10.1016/j.quascirev.2016.02.015>

198 Frezzotti, M., Urbini, S., Proposito, M., Scarchilli, C., Gandolfi, S. (2007). Spatial and temporal variability of surface  
199 mass balance near Talos Dome, East Antarctica. *Journal of Geophysical Research* 112, F02032.

200 Gilbert, D., Freundt, A., Kutterolf, S. et al. (2014) Post-glacial time series of explosive eruptions and associated  
201 changes in the magma plumbing system of Lonquimay volcano, south central Chile. *International Journal of Earth*  
202 *Sciences* 103, 2043–2062, <https://doi.org/10.1007/s00531-012-0796-x>

203 Jochum, K.P., Dingwell, D.B., Rocholl, A., Stoll, B., Hofmann, A.W., Becker, S., Besmehn, A., Bessette, D., Dietze, H.,  
204 Dulski, P., Erzinger, J., Hellebrand, E., Hoppe, P., Horn, I., Janssens, K., Jenner, G., Klein, M., McDonough, W. Maetz,  
205 M., Mezger, K., Mürker, C., Nikogosian, I., Pickhardt, C., Raczek, I., Rhede, D., Seufert, H., Simakin, S., Sobolev, A.,  
206 Spettel, B., Straub, S., Vincze, L., Wallianos, A., Weckwerth, G., Weyer, S., Wolf, D., Zimmer, M. (2000). The  
207 Preparation and Preliminary Characterisation of Eight Geological MPI-DING Reference Glasses for In-Situ  
208 Microanalysis. *Geostandards Newsletter* 24: 87-133, doi:10.1111/j.1751-908X.2000.tb00590.x

209  
210 Hall, M., Mothes, P. (2008). The rhyolitic-andesitic eruptive history of Cotopaxi volcano, Ecuador. *Bulletin of*  
211 *Volcanology* 70, 675-702.

- 212 Koffman, B.G., Dowd, E.G., Osterberg, E.C., Ferris, D.G., Hartman, L.H., Wheatley, S.D., et al. (2017). Rapid transport  
213 of ash and sulfate from the 2011 Puyehue-Cordón Caulle (Chile) eruption to West Antarctica. *Journal of Geophysical*  
214 *Research: Atmospheres* 122, 8908-8920, <https://doi.org/10.1002/2017JD026893>
- 215 Kratzmann, D.J., Carey, S., Scasso, R., Naranjo, J.A. (2009). Compositional variations and magma mixing in the 1991  
216 eruptions of Hudson volcano, Chile. *Bulletin of Volcanology* 71, 419-439, doi:10.1007/s00445-008-0234
- 217 Kraus, S., Kurbatov, A., Yates, M. (2013). Geochemical signatures of tephras from Quaternary Antarctic Peninsula  
218 volcanoes: *Andean Geology* 40 (1), 1-40, doi:<http://dx.doi.org/10.5027/andgeoV40n1-a01>
- 219 Kutterolf, S., Freundt, A. & Burkert, C. (2011). Eruptive history and magmatic evolution of the 1.9 kyr Plinian dacitic  
220 Chiltepe Tephra from Apoyeque volcano in west-central Nicaragua. *Bulletin of Volcanology* 73, 811-831,  
221 doi:10.1007/s00445-011-0457-0
- 222 Lavallée, Y., de Silva, S.L., Salas, G., Byrnes, J.M. (2006). Explosive volcanism (VEI 6) without caldera formation:  
223 insight from Huaynaputina volcano, southern Peru. *Bulletin of Volcanology* 68, 333-348, DOI 10.1007/s00445-005-  
224 0010-0
- 225 Lavigne, F., Degeai, J.-P., Komorowski, J.-C., Guillet, S., Robert, V., Lahitte, P., Oppenheimer, C., Stoffel, M., Vidal,  
226 C.M., Surono, Pratomo, I., Wassmer, P., Hajdas, I., Sri Hadmoko, D., de Belizal, D., (2013). Source of the great A.D.  
227 1257 mystery eruption unveiled, Salamas volcano, Rinjani Volcanic Complex, Indonesia. *Proceedings of the*  
228 *National Academy of Sciences* Sep 2013, 201307520; DOI: 10.1073/pnas.1307520110
- 229 Mehringer, P.J. Jr., Sarna-Wojcicki, A.M., Wollwage, L.K., Sheets, P. (2005). Age and extent of the Ilopango TBJ  
230 Tephra inferred from a Holocene chronostratigraphic reference section, Lago De Yojoa, Honduras. *Quaternary*  
231 *Research* 63(2), 199-205, <https://doi.org/10.1016/j.yqres.2004.09.011>  
232
- 233 Metrich, N., Rutherford, M.J. (1992). Experimental study of chlorine behavior in hydrous silicic melts. *Geochimica et*  
234 *Cosmochimica Acta*, 56 (2), 607-616, [https://doi.org/10.1016/0016-7037\(92\)90085-W](https://doi.org/10.1016/0016-7037(92)90085-W)  
235
- 236 Moreno, P.I., Alloway, B.V., Villarosa, G., Outes, V., Henríquez, W.I., De Pol-Holz, R., Pearce, N.J.G. (2015). A past-  
237 millennium maximum in postglacial activity from Volcán Chaitén, southern Chile. *Geology* 43, 47-50,  
238 doi:10.1130/G36248.1  
239
- 240 Morgan, G.B., London, D. (1996). Optimizing the electron microprobe analysis of hydrous alkali aluminosilicate  
241 glasses. *American Mineralogist* 81 (9-10), 1176-1185, DOI: <https://doi.org/10.2138/am-1996-9-1016>  
242
- 243 Nairn, I.A, Shane, P.R, Cole, J.W, Leonard, G.J., Self, S., Pearson, N. (2004). Rhyolite magma processes of the ~AD  
244 1315 Kaharoa eruption episode, Tarawera volcano, New Zealand. *Journal of Volcanology and Geothermal Research*  
245 131 (3-4), 265-294, [https://doi.org/10.1016/S0377-0273\(03\)00381-0](https://doi.org/10.1016/S0377-0273(03)00381-0)
- 246 Naranjo, J., Moreno, H., Emparan, C., Murphy, M. (1993). Volcanismo explosivo reciente en la caldera del volcan  
247 Sollipulli, Andes del Sur (39°S). *Revista Geológica de Chile* 20 (2), 167-191,  
248 doi:<http://dx.doi.org/10.5027/andgeoV20n2-a03>
- 249 Narcisi, B., Petit, J.R., Delmonte, B. (2010). Extended East Antarctic ice core tephrostratigraphy. *Quaternary Science*  
250 *Reviews* 29, 21-27.
- 251 Narcisi, B., Petit, J.R., Delmonte, B., Scarchilli, C., Stenni, B. (2012). A 16,000-yr tephra framework for the Antarctic  
252 ice sheet: a contribution from the new Talos Dome core. *Quaternary Science Reviews* 49, 52-63.
- 253 Narcisi, B., Petit, J.R., Langone, A., Stenni, B. (2016). A new Eemian record of Antarctic tephra layers retrieved from  
254 the Talos Dome ice core (Northern Victoria Land). *Global and Planetary Change* 137, 69-78,  
255 <http://dx.doi.org/10.1016/j.gloplacha.2015.12.016>
- 256 Nielsen, S.H.H., Hodell, D.A., Kamenov, G., Guilderson, T., Perfit, M.R. (2007). Origin and significance of ice-rafted  
257 detritus in the Atlantic sector of the Southern Ocean, *Geochemistry, Geophysics, Geosystems* 8, Q12005,

- 258 doi:10.1029/2007GC001618
- 259 Nielsen, C.H., Sigurdsson, H. (1981). Quantitative methods for electron micro-probe analysis of sodium in natural  
260 and synthetic glasses. *American Mineralogist* 66, 547-552.
- 261
- 262 Nooren, K., Hoek, W.Z., van der Plicht, H., Sigl, M., van Bergen, M.J., Galop, D., Torrescano-Valle, N. et al. (2017).  
263 Explosive eruption of El Chichón volcano (Mexico) disrupted 6<sup>th</sup> century Maya civilization and contributed to global  
264 cooling. *Geology* 45, 175-178, doi:10.1130/G38739.1
- 265
- 266 Osipov, E.Y., Khodzher, T.V., Golobokova, L.P., Onischuk, N.A., Lipenkov, V.Y., Ekaykin, A.A., Shibaev, Y.A., Osipova,  
267 O.P. (2014). High-resolution 900 year volcanic and climatic record from the Vostok area, East Antarctica. *The*  
268 *Cryosphere* 8, 843-851.
- 269 Palais, J.M., Germani, M.S., Zielinski, G.A. (1992). Interhemispheric transport of volcanic ash from a 1259 A.D.  
270 volcanic eruption to the Greenland and Antarctic ice sheets. *Geophysical Research Letters* 19(8), 801-804.
- 271 Pitts, M.C., Thomason L.W. (1993). The impact of the eruptions of Mount Pinatubo and Cerro Hudson on Antarctic  
272 aerosol levels during the 1991 austral spring. *Geophysical Research Letters* 20, 2451-2454,  
273 <https://doi.org/10.1029/93GL02160>
- 274 Rawson, H., Naranjo, J.A., Smith, V.C. Fontijn, K., Pyle, D.M., Mather, T.A., Moreno, H. (2015). The frequency and  
275 magnitude of post-glacial explosive eruptions at Volcán Mocho-Choshuenco, southern Chile. *Journal of*  
276 *Volcanology and Geothermal Research* 299, 103-129.
- 277 Ruprecht P., Bergantz, G.W., Cooper, K.M., Hildreth, W. (2012). The Crustal Magma Storage System of Volcán  
278 Quizapu, Chile, and the Effects of Magma Mixing on Magma Diversity. *Journal of Petrology* 53 (4), 801-840,  
279 <https://doi.org/10.1093/petrology/egs002>
- 280 Shane, P.A.R., Froggatt, P.C. (1992). Composition of widespread volcanic glass in deep-sea sediments of the  
281 Southern Pacific Ocean: an Antarctic source inferred. *Bulletin of Volcanology* 54, 595-601.
- 282
- 283 Schindlbeck, J.C., Kutterolf, S., Freundt, A., Alvarado, G.E., Wang, K.-L., Straub, S.M., Hemming, S.R., Frische, M.,  
284 Woodhead J.D. (2016). Late Cenozoic tephrostratigraphy offshore the southern Central American Volcanic Arc: 1.  
285 Tephra ages and provenance, *Geochemistry, Geophysics, Geosystems* 17, 4641-4668, doi:10.1002/2016GC006503
- 286 Schwander, J., Jouzel, J., Hammer, C.U., Petit, J.R., Udisti, R., Wolff, E. (2001). A tentative chronology for the EPICA  
287 Dome Concordia ice core. *Geophysical Research Letters* 28 (22), 4243-4246.
- 288 Severi, M., Udisti, R., Becagli, S., Stenni, B., Traversi, R. (2012). Volcanic synchronisation of the EPICA-DC and  
289 TALDICE ice cores for the last 42 kyr BP. *Climate of the Past* 8, 509-517.
- 290 Singer, B.S., Thompson, R.A. Dungan, M.A., Feeley, T.C., Nelson S.T., Pickens, J.C., Brown, L.L., Wulff, A.W., Davidson,  
291 J.P., Metzger, J. (1997). Volcanism and erosion during the past 930 k.y. at the Tatara-San Pedro complex, Chilean  
292 Andes. *Geological Society of America Bulletin* 109 (2), 127-142.
- 293
- 294 Spray, J.G., Rae, D.A. (1995). Quantitative electron-microprobe analysis of alkali silicate-glasses: A review and user  
295 guide. *Canadian Mineralogist* 33, 323-332.
- 296
- 297 Stern, C.R. (2008). Holocene tephrochronology record of large explosive eruptions in the southernmost Patagonian  
298 Andes. *Bulletin of Volcanology* 70, 435-454.
- 299 Stewart A.-M., Castro J.M. (2016). P-T-X evolution of the 1280 AD Quilotoa dacite. *Journal of Volcanology and*  
300 *Geothermal Research* 313, 29-43, <https://doi.org/10.1016/j.jvolgeores.2015.11.024>
- 301 Thouret, J.-C., Finizola, A., Fornari, M., Legeley-Padovani, A., Suni, J., Frechen, M. (2001). Geology of El Misti volcano  
302 near the city of Arequipa, Peru. *Geological Society of America Bulletin* 113, 1593-1610.

- 303 Vidal, C.M., Komorowski, J.-C., Metrich, N., Pratomo, I., Kartadinata, N., Prambada, O., Michel, A., Carazzo, G.,  
304 Lavigne, F., Rodysill, J., Fontijn, K., Surono (2015). Dynamics of the major plinian eruption of Samalas in 1257 A.D.  
305 (Lombok, Indonesia). *Bulletin of Volcanology* 77, 73. DOI 10.1007/s00445-015-0960-9
- 306 Vidal, C.M., Metrich, N., Komorowski, J.-C., Pratomo, I., Michel, A., Kartadinata N., Vincent R., Lavigne, F. (2016). The  
307 1257 Samalas eruption (Lombok, Indonesia): the single greatest stratospheric gas release of the Common Era.  
308 *Scientific Reports* 6, Article number: 34868, DOI: 10.1038/srep34868
- 309 Watt, S.F.L., Pyle, D.M., Naranjo, J., Rosqvist, G., Mella, M., Mather, T.A., Moreno, H. (2011). Holocene  
310 tephrochronology of the Hualaihue region (Andean southern volcanic zone, ~ 42°S), southern Chile. *Quaternary*  
311 *International* 246, 324-343, <http://dx.doi.org/10.1016/j.quaint.2011.05.029>